November 30th, 2022

Constraining flow and sediment transport intermittency in the geological past

Sinéad J. Lyster[1,2,*], Alexander C. Whittaker[2], Alex Farnsworth[3] and Gary J. Hampson[2]

[1]Department of Geosciences, The Pennsylvania State University, Pennsylvania, USA.
[2]Department of Earth Science and Engineering, Imperial College London, UK.
[3]School of Geographical Sciences and Cabot Institute, University of Bristol, UK.
*slyster@psu.edu

Abstract

Quantitative investigations of ancient rivers usually provide insights into either instantaneous or mean flow conditions. There is a critical gap between these timescales of investigation which reflects the intermittency of flow and sediment transport, and closing this gap is crucial to fully explore the dynamics and evolution of ancient fluvial landscapes. Here, we combine fluvial stratigraphic datasets, flow and sediment transport models, and paleoclimate general circulation model (GCM) results to develop new methods to estimate intermittency in the geological past, specifically flow intermittency factors (I_w) and sediment transport intermittency factors (I_s). We illustrate these methods for the Upper Cretaceous Last Chance Ferron Sandstone, Utah, USA. For sand-transporting flow conditions in Last Chance Ferron rivers, we estimate I_w values of $0.54-0.90$, which imply that channel-forming flows were sustained for the majority of the year, consistent with perennial systems in which relatively large discharges are sustained. In contrast, for gravel-transporting flow conditions, I_w values of $0.28-0.38$ suggest that the largest formative flows may have occupied Last Chance Ferron rivers for nearly a third of the year, which could be explained by a monsoonal system in which high magnitude discharge events are sustained, or a subtropical system in which high magnitude discharge events have short durations but high frequencies. Meanwhile, I_s values of $0.075-0.15$ suggest that annual sediment budgets could have been transported in as little as 10 days, but up to 2 months, if channel-forming conditions were sustained, and highlight that small changes to the duration of channel-forming conditions could significantly impact sediment budgets. These results are consistent with independent facies- and proxy-based insights into Last Chance Ferron rivers, which point to a perennially wet system characterized by a monsoonal or subtropical discharge regime. Our results highlight new opportunities to use paleoclimate GCMs to constrain intermittency in the geological past. Going forward, paleoclimate GCMs will be particularly useful where the rock record is incomplete or inaccessible, or where stratigraphic approaches are limited, and will enable us to tackle pertinent research questions pertaining to past surface processes on both Earth and other planets.

1. Introduction

Quantitative investigations of ancient fluvial systems can provide insights into either instantaneous or mean flow conditions in the geological past. Field-based stratigraphic approaches to reconstruct river dynamics often recover instantaneous channel-forming conditions, such as water discharges or sediment transport capacities at a particular point in time or space (Holbrook & Wanas, 2014; Lin & Bhattacharya, 2017; Sharma et al., 2017; Ganti et al., 2019; Lyster et al., 2021). In contrast, catchment and regional-scale models of ancient sediment routing systems tend to recover mean annual conditions, or mean conditions on longer, million-year timescales (Allen et al., 2013; Stephenson et al., 2014; Watkins et al., 2018b; Fernandes et al., 2019; Lyster et al., 2020). There is a critical gap between these timescales of investigation which reflects the intermittency of flow and sediment transport. At present, this gap is difficult to reconcile.

The intermittency of a river describes the temporal distribution of flow and sediment transport. Two endmembers can be defined: a highly intermittent system is characterised by multiple and/or sustained periods of zero flow or sediment transport, whereas a non-intermittent system is characterised by persistent

flow or sediment transport. For geological applications, Paola et al. (1992) introduced a dimensionless intermittency factor, with a value between zero and one, as a simple method of time averaging when using instantaneous sediment transport equations to investigate sediment fluxes and basin infilling on longer geological timescales. The selected averaging time must be long relative to individual channel-forming events (instantaneous conditions) but short relative to longer geological timescales (mean conditions), and the simplest method is to assume that flow is characterized by a series of channel-forming conditions that occur intermittently (Paola et al., 1992). Channel-forming conditions that produce fluvial strata are commonly taken as bankfull and/or flood conditions (Wolman & Miller, 1960; Dunne & Leopold, 1978), but could feasibly reflect ordinary flow conditions (Ganti et al., 2014; Paola et al., 2018; Ganti et al., 2020; Holbrook & Miall, 2020). The intermittency factor represents the sum of these channel-forming conditions, and is formally defined as the fraction of a chosen time period that is required for a constant channel-forming flow to transport the same amount of water or sediment as the river hydrograph actually does over the chosen time period (Paola et al., 1992). This means the intermittency factor reflects the time-dependent integral of the river hydrograph (Figure 1). It does not directly constrain the specific distribution of individual flow events — different hydrographs could have similar intermittency factors (Figure 1).

Constraints on intermittency factors are crucial to upscale estimates of instantaneous conditions to mean conditions, or *vice versa*, and, therefore, reconstruct the flux of water, sediment, and nutrients across Earth's surface in the geological past (Hilton et al., 2008; Goñi et al., 2013; Holbrook & Wanas, 2014; Leithold et al., 2016; Lin & Bhattacharya, 2017; Sharma et al., 2017). However, to date, assumptions of intermittency factors in ancient rivers are often based on empirical observations of potentially analogous modern rivers, and these assumptions have large uncertainty margins (e.g., Meybeck et al., 2003). Developing methods to constrain intermittency factors in the geological past therefore remains a prominent research challenge.

Here we present new methods to estimate intermittency factors in the geological past, which incorporate fluvial stratigraphic datasets, flow and sediment transport models, and paleoclimate general circulation model (GCM) results, and we illustrate these methods for a Late Cretaceous fluvial system in Utah, USA. Our results highlight the potential to use multidisciplinary datasets to constrain intermittency factors. Further, we show how to use these constraints, in conjunction with independent insights from facies observations and terrestrial paleoclimate proxies, to explore past hydrograph shapes (Figure 1). Consequently, our results have important implications for reconstructing the magnitudes and characteristics of past flood events (Chen et al., 2018), and for reconstructing river behavior as a function of different (paleo)climates (Lyster et al., 2020; Lyster et al., 2021) and climate perturbation (Foreman et al., 2012; Chen et al., 2018; Pujalte et al., 2022). Our results help to close the gap between instantaneous and mean timescales of investigation, providing new insights into the transport of water and mass across Earth's surface in the geological past. Going forward, we suggest that paleoclimate GCMs will be particularly useful for investigating intermittency factors where the rock record is incomplete or inaccessible and will provide new insights into past surface processes on both Earth and other terrestrial planetary bodies.

2. Research background
2.1 Constraining flow intermittency

While the intermittency factor was introduced as a sediment transport intermittency factor (Paola et al., 1992), we can consider a flow intermittency factor as the simplest expression of this concept (Figure 1). The flow intermittency factor, I_w, is the fraction of the total time that a river could transport the same amount of water at channel-forming conditions as it transports during the real hydrograph (Paola et al., 1992). I_w can be expressed as:

$$I_w = \frac{\sum Q_w(t)}{Q_{w(cf)} \sum t}$$

Eq. 1

where Q_w is water discharge, $Q_{w(cf)}$ is channel-forming water discharge, $\sum Q_w(t)$ is the sum of the time dependent water discharge, and $\sum t$ is the timespan. For example, if $\sum t=1$ year, then $\sum Q_w(t)$ reflects the sum of water discharge over a 1-year period (i.e., the annual water budget) and $Q_{w(cf)}\sum t$ reflects the theoretical water discharge for the same 1-year period if channel-forming conditions are sustained (Figure 1a). When calculated like this, intermittency factors assume that channel-forming conditions do all the geomorphic work and, therefore, inherently assume that the remainder of the hydrograph is characterized by zero flow, or by low flow conditions that do no geomorphic work (Figure 1a). In reality, this assumption is rarely applicable. In most rivers, a given intermittency factor can manifest as a number of possible hydrograph shapes (Figure 1b–d). Here we show that flow intermittency factors, when used in conjunction with facies-based insights into flow intermittency, can be used to narrow down potential hydrograph shapes (Figure 1b–d).

Facies-based insights into flow intermittency can be gained from fluvial strata. Flow intermittency is not synonymous with flow variability, which can refer to unsteady/nonuniform flow on a variety of temporal and spatial scales, including annual–decadal, seasonal–interannual, near-instantaneous, and instantaneous timescales, and regional, catchment, and reach spatial scales (Table 1). However, as intermittency factors reflect the integral of the river hydrograph, we suggest that flow intermittency factors most closely reflect seasonal–interannual flow variability at catchment-scales (Table 1). At these timescales, insights into flow variability typically arise from variable discharge facies models, in which potentially distinctive sedimentary structures are used to discriminate highly variable (i.e., monsoonal/subtropical) and less variable (i.e., perennial) discharge systems (Fielding et al., 2009; Plink-Björklund, 2015; Gall et al., 2017; Fielding et al., 2018; Birgenheier et al., 2019; Herbert et al., 2020; Wang & Plink-Björklund, 2020). Another, albeit less direct, approach is to assess surface runoff regime from fluvial strata. The presence of coals, evaporites, and paleosols can be attributed to specific runoff regimes and used to determine whether deposition occurred in wet, humid, semi-arid, or arid climates (Parrish et al., 1982; Parrish & Barron, 1986; McCabe & Parrish, 1992; Mack & James, 1994; Bestland et al., 1997; Tabor et al., 2008; Tabor & Myers, 2014). Runoff regime is intrinsically linked with discharge regime and may therefore provide insights into the temporal distribution of flow.

Variable discharge and surface runoff facies models provide useful insights into flow variability and, by proxy, flow intermittency, however these models are limited. For example, depositional features associated with surface runoff facies are not controlled by runoff alone — these features are climatically sensitive and can occur as a function of temperature and evaporation, as well as water table depth. Further, these models do not provide quantitative constraints on flow intermittency, which limits interpretation.

2.2 Constraining sediment transport intermittency

Sediment transport intermittency factors offer insights into the timespans over which fluvial systems redistribute sediment (Figure 1). The sediment transport intermittency factor, I_s, is the fraction of time that a river could transport the same amount of sediment at channel-forming conditions as it transports during the real hydrograph for a given time interval (Paola et al., 1992) — this inherently assumes that all sediment is transported during channel-forming conditions (Wolman & Miller, 1960). Like Equation 1, I_s can be expressed as:

$$I_s = \frac{\sum Q_s(t)}{Q_{s(cf)} \sum t}$$

Eq. 2

where Q_s is sediment flux, $Q_{s(cf)}$ is channel-forming sediment flux, $\sum Q_s(t)$ is the sum of the time dependent sediment flux, and $\sum t$ is the timespan. If $\sum t=1$ year, then $\sum Q_s(t)$ reflects the sum of sediment flux over a 1-year period (i.e., the annual sediment budget), and $Q_{s(cf)}\sum t$ reflects the theoretical annual sediment budget for the same 1-year period if channel-forming conditions are sustained (Figure 1e).

Sediment transport intermittency factors are not necessarily proxies for flow intermittency factors; one river may transport its entire annual sediment load during a yearly flood (Figure 1e), whereas another may transport sediment all year round (Figure 1f–h). Consequently, I_s is usually less than I_w. Sediment transport intermittency is only a proxy for flow intermittency in rivers that transport their entire water and sediment budget during channel-forming conditions (Figure 1e), such as very flashy ephemeral rivers. Nonetheless, sediment transport intermittency constraints are useful complements to flow intermittency constraints and are necessary to understand mass transport across Earth's surface in the geological past. In catchments with high erosional thresholds, annual sediment budgets may be determined by the frequency of threshold-surpassing events, e.g., storms. In these systems, small changes to sediment transport intermittency driven by, e.g., enhanced storminess, could result in major changes to annual sediment budgets (e.g., Romans et al., 2016). Therefore, constraints on sediment transport intermittency encode information on fluvial sensitivity to climate perturbation.

Sediment transport intermittency factors have been increasingly documented in modern rivers (e.g., Meybeck et al., 2003; Sklar & Dietrich, 2004; Wright & Parker, 2005; Czuba & Foufoula-Georgiou, 2014; Hayden et al., 2021a) and, in some instances, have been correlated with catchment parameters, e.g., drainage area (Meybeck et al., 2003), and applied to ancient systems to upscale estimates of instantaneous sediment fluxes to mean annual sediment fluxes (Holbrook & Wanas, 2014; Lin & Bhattacharya, 2017; Sharma et al., 2017). However, the predictive capability of these correlations is low (Meybeck et al., 2003). Recent work sought correlation between sediment transport intermittency factors and alternative parameters, e.g., bed material grain size and climate aridity, but found they were uncorrelated (Hayden et al., 2021a).

Alternatively, stratigraphic techniques can be used to estimate sediment transport intermittency in ancient rivers. These techniques include using estimates of sediment fluxes to calculate the minimum time required to accumulate a given sediment volume — this approach is regularly used to investigate minimum formation timescales of ancient depositional systems in planetary examples such as Mars (Moore et al., 2003; Jerolmack et al., 2004; Bhattacharya et al., 2005; Kleinhans, 2005; Metz et al., 2009). Where sediment volumes are age-constrained, or where timespans of fluvial activity (including periods of inactivity) can be estimated, the sediment transport intermittency can be calculated (Buhler et al., 2014; Lapôtre & Ielpi, 2020; Hayden et al., 2021b). It is important to note that this approach is limited by the incomplete nature of the rock record, notably periods of erosion (e.g., Sadler, 1981; Sadler, 1993), and requirement of a mass balance assumption.

2.3 New opportunities to constrain flow and sediment transport intermittency

To constrain intermittency in the geological past, we require estimates of both instantaneous channel forming flow conditions (which reflect $Q_{w(cf)}$ and $Q_{s(cf)}$ in Equations 1 and 2) and mean flow conditions (which reflect $\sum Q_w(t)$ and $\sum Q_s(t)$ in Equations 1 and 2) for the same depositional systems. With detailed field measurements of channel geometries and grain-size from fluvial strata, we can implement flow and sediment transport models to reconstruct instantaneous water discharges and sediment fluxes in ancient rivers (e.g., Engelund & Hansen, 1967; van Rijn, 1984; García & Parker, 1991; Wright & Parker, 2004; Mahon & McElroy, 2018). Further, where associated depositional volumes have robust age constraints, reconstructed sediment fluxes can be used to estimate sediment transport intermittency factors (e.g., Hayden et al., 2021b). This approach is increasingly useful given an ever-expanding repertoire of methods to reconstruct channel morphologies from fluvial strata, many of which are now incorporated into frameworks that carefully consider uncertainty (e.g., Ganti et al., 2019; Greenberg et al., 2021; Hayden et al., 2021b; Lyster et al., 2021; Lyster et al., 2022a; Lyster et al., 2022b; Wood et al., 2022).

Advances in paleoclimate modelling simultaneously provide new opportunities to estimate paleoflow conditions. Lyster et al. (2020) presented a new approach that uses paleoclimate GCM results to estimate water discharges and sediment fluxes in ancient catchments. Their approach exploited high resolution

paleo-topographic reconstructions that had been digitised as paleo-digital elevation models (Markwick & Valdes, 2004; Markwick, 2018). Where the sizes and configurations of paleo-catchments are well-understood, and where the positions and approximate elevations of orogens are known, Lyster et al. (2020) showed that paleoclimate GCM results (e.g., Farnsworth et al., 2019a) and the BQART suspended sediment flux model (Syvitski & Milliman, 2007) can be used to make first order approximations of mean water discharges and sediment fluxes in paleo-catchments.

Here we take fluvial stratigraphic data, which comprise detailed field measurements, and paleoclimate GCM results, which were derived using the HadCM3L GCM (Farnsworth et al., 2019a), and we combine these datasets with the aforementioned research frameworks to present new approaches to constrain intermittency in the geological past.

3.   Geologic Setting

We focus on deposits of the Ferron Sandstone, which provide the preserved record of Turonian (Late Cretaceous) coastal depositional systems in Utah, USA (Figures 2–4). Specifically, we focus on the Last Chance fluvio-deltaic system of the Ferron Sandstone, which was fed by a major river that drained the Sevier mountains toward the Western Interior Seaway (WIS) (Cotter, 1975a, 1975b, 1976; Chidsey et al., 2004), and which may have featured a longitudinal component of drainage from the south-southwest (Kynaston, 2019) (Figure 2).

Deposits of the Last Chance fluvio-deltaic system crop out in central Utah and extend southwest−northeast over a length of ~65 km (Figures 2, 3). In the southwest (paleo-landward), deposits comprise terrestrial fluvial facies, and to the northeast (paleo-seaward), deposits grade into deltaic facies (Figure 3). We collected field data from the most paleo-landward deposits (Figures 2, 3), where channelized fluvial sandstone bodies are surrounded by abundant floodplain fines, including paleosols and coals (Figures 3, 4). Channelized sandstone bodies preserve major meandering trunk channels, as evidenced by abundant laterally accreted point bar deposits (Cotter, 1971; Bhattacharya & Tye, 2004) (Figure 4c) — this interpretation is consistent with that of the trunk channel that fed the neighbouring Notom fluvio-deltaic system of the Ferron Sandstone (Fielding, 2010; Bhattacharyya et al., 2015; Wu et al., 2015; Li et al., 2018).

The Last Chance Ferron system is particularly suitable as an exemplar to test methods to constrain intermittency for four reasons. First, extensive outcrop enables detailed field investigation; constraints on channel geometries can be readily obtained which facilitates reconstruction of water discharges and sediment fluxes. Second, depositional sequence stratigraphy is well-documented (Garrison Jr et al., 1997; Anderson & Ryer, 2004; Gardner et al., 2004; Garrison Jr & van den Bergh, 2004; van den Bergh & Garrison, 2004), which facilitates estimation of the preserved depositional volume (Figure 3). Third, the age and timespan is well-constrained; Garrison Jr and van den Bergh (2004) determined that the Last Chance Ferron Sandstone was deposited over a period of 1.7 million years (90.3−88.6 Ma) using biostratigraphic and stratigraphic correlation charts which they calibrated using $^{40}Ar/^{39}Ar$ isotopic data (Molenaar & Cobban, 1991; Kauffman & Caldwell, 1993; Obradovich, 1993; Gardner, 1995; Shanley & McCabe, 1995). Fourth, we require a mass balance assumption, i.e., that, for a given time interval, the sediment volume passing through a trunk channel cross section is equal to both the sediment volume contributed by the source region and the sediment volume deposited in the sink region. This assumption is crucial when comparing estimates of sediment fluxes with preserved depositional volumes. Here, the interpretation that a major single-thread trunk channel fed the Last Chance delta (Figure 2b), and that the depositional volume is predominantly complete (Figure 3), enables this assumption. This assumption is difficult to justify in systems where depositional volumes are significantly incomplete, or in systems involving multi-thread rivers and/or fluvial fans, which would require knowledge of the number and geometries of all active channels.

4. Methods

We used field measurements to estimate channel geometries, and a series of flow and sediment transport models to estimate instantaneous channel-forming water discharges, $Q_{w(cf)}$, and bed material loads, $Q_{bm(cf)}$, in Last Chance Ferron rivers. Then, we used paleoclimate GCM results to estimate mean annual Q_w and mean annual suspended sediment flux, Q_s. With these estimates, and with estimates of the Last Chance Ferron depositional volume, we calculated flow intermittency factors, I_w, and sediment transport intermittency factors, I_s, for Last Chance Ferron rivers using Equations 1 and 2.

To account for variability and/or uncertainty in model inputs and parameters we implemented a Monte Carlo scheme. For each model input and parameter in Equations 1–8 (and Equations S1–S14), we implemented a range of values. In most instances, we determined this range using the mean (μ) and standard deviation (σ) of the field, topographic, and paleoclimatic data described in the following sections. Using this range, we randomly sampled 10^6 values from a uniform distribution, and we propagated these 10^6 values throughout Equations 1–8 (and Equations S1–S14) and recovered 10^6 plausible values for I_w and I_s.

Our methods are synthesised below, and a complete account of every workflow step, including further details of the uncertainty analysis, is presented in the supplement.

4.1 Field-derived estimates of paleoflow conditions
    i.   Field methods

In channelized fluvial sandstones, we measured thicknesses and grain-sizes of individual cross-sets in channel-fill facies and the heights of channel architectural elements (Figure 4). For individual cross-sets (n=190) we measured cross-set thickness, h_{xs}, at regular intervals along the cross-set width, and we combined all h_{xs} measurements (n=1485) and extracted μ and σ for these data (Table 2). For each cross-set we also estimated the median grain-size, D_{50}, (n=190) using grain-size cards and the Wentworth (1922) classification, and we similarly combined all D_{50} values and extracted μ and σ (Table 2). Finally, we measured channel architectural elements which, where fully preserved, are a proxy for flow depth (e.g., Hajek & Heller, 2012). We primarily measured barform-scale clinoform (accretion) heights, but additionally measured maximum thicknesses of single channel storeys and compiled existing data from literature (n=51; see Supplement). We also extracted μ and σ for these data (Table 2).

We collected field data throughout terrestrial fluvial strata of the Last Chance Ferron Sandstone, and we therefore assumed that these data reflect channel-forming conditions in Last Chance Ferron rivers. While channel-forming conditions are often attributed to bankfull flows, this is not necessarily true. Channel-fill deposits were predominantly sand-grade, and we therefore assumed that sand-transporting flow conditions were the dominant channel-forming condition. We proceeded to calculate sand-transporting flow conditions and intermittency factors using a range of field data inputs bounded by μ−σ and μ+σ (Table 2).

In some instances, poorly sorted gravel-grade lenses and horizons (usually <50 cm thick) were present in channel-fill deposits (Figure 4d, g, h). We assumed that gravel-grade fractions reflect the largest flow conditions preserved in the stratigraphy, but that these were not the dominant channel-forming condition. To capture data that potentially reflect the largest flow conditions, we established grain size distributions of each lens or horizon using the Wolman (1954) point count method (n=8 counts; ~100 measurements per count). We then combined all gravel grain size measurements and extracted μ and σ (Table 2). To simulate the largest flow conditions, we proceeded to calculate gravel-transporting flow conditions and intermittency factors using a range of field data inputs bounded by μ and μ+σ (Table 2).

    ii.   Channel geometries

To estimate channel geometries, we used h_{xs} and a range of plausible bedform preservation ratios (0.3−0.7; Table 2) to estimate original dune heights, h_d. Then, we used channel architectural element heights as proxies

for flow depths, H (Table 2) — these estimates are corroborated by independent approaches to estimate H (see Supplement). Using D_{50} and H, we estimated slope, S, using the widely-used empirical relation of Trampush et al. (2014) (Equation S1). The final channel geometrical parameter we required was width, W, which, for Last Chance Ferron rivers, has previously been constrained from outcrop. Bhattacharya and Tye (2004) and Garrison Jr and van den Bergh (2004) reported valley-scale trunk channels with a mean W of 250 m, and Garrison Jr and van den Bergh (2004) found no evidence to suggest that W exceeded a few hundred metres, and noted that measured channel-belt widths did not exceed 2 km. To allow for uncertainty, we implemented $W = 200-300$ m.

iii.   Flow conditions

We calculated instantaneous channel-forming water discharge, $Q_{w(cf)}$, as:

$$Q_{w(cf)} = UHW, \qquad \text{Eq. 3}$$

where U is the flow velocity, which we calculated using Chézy formulae (Equations S2 and S3), and where H and W were determined from primary and secondary field data.

To calculate the instantaneous channel-forming bed material load, $Q_{bm(cf)}$, we first calculated the bedload fraction of the bed material load, $Q_{bm(b)}$, using the relation of Mahon and McElroy (2018), a bedform-scale approach in which bedload is calculated geometrically, per unit width. In this relation, $Q_{bm(b)}$ is calculated as:

$$Q_{bm(b)} = (1 - \varphi)\frac{h_d V_c}{2}, \qquad \text{Eq. 4}$$

where φ is a dimensionless bed porosity of 0.5 and V_c is the characteristic bedform migration velocity (also calculated following Mahon and McElroy (2018); Equation S12). Next, we calculated the suspended fraction of the bed material load, $Q_{bm(s)}$, using the entrainment relation and form drag predictor of Wright and Parker (2004), where:

$$Q_{bm(s)} = \frac{u_* E H}{\kappa}I, \qquad \text{Eq. 5}$$

and where $u*$ is the bed shear velocity, E is entrainment of uniform material (effectively the concentration of suspended sediment at a reference height or level), κ is the von Karman constant, taken as 0.4, and I is the Rouse–Vanoni profile for suspended sediment (see Supplement).

With estimates of both $Q_{bm(b)}$ and $Q_{bm(s)}$ for channel-forming conditions, we calculated $Q_{bm(cf)}$ as:

$$Q_{bm(cf)} = Q_{bm(b)} + Q_{bm(s)}. \qquad \text{Eq. 6}$$

Our methods to calculate $Q_{w(cf)}$ and $Q_{bm(cf)}$ are fully detailed in the Supplement, including how we calculated U, V_c, $u*$, E, and I.

4.2 GCM-derived estimates of paleoflow conditions
i.   Paleo-catchment geometries and climate

To derive paleoflow conditions using paleoclimate GCM results, we require approximate constraints on paleo-catchment geometries. For the Late Cretaceous Western Interior, particularly the western margin of the WIS, detailed understanding of paleogeography enables us to place reasonable bounds on the drainage area, A, and maximum relief, R, of the Last Chance Ferron paleo-catchment. Prior knowledge includes constraints on the position of the paleo-shoreline and the distance to the Sevier highlands (Figure 5a, b;

Kauffman (1977); Hay et al. (1993); Kauffman and Caldwell (1993); Roberts and Kirschbaum (1995)), theory of catchment outlet spacing (Hovius, 1996), published paleogeographic reconstructions (Gardner, 1995; Bhattacharya & Tye, 2004; Ryer & Anderson, 2004; Bhattacharya et al., 2016; Kynaston, 2019), and previous reconstructions of paleo-catchment configurations from paleo-digital elevation models (c.f. Lyster et al. (2020)). As such, we know that the Last Chance Ferron trunk channel drained an area of order 10^4 km², and we can narrow this range to A=25,000–35,000 km² (Figure 5b; Table 2). Meanwhile, topographic relief in the Sevier mountains has been described as "Andean" in scale with mean elevations exceeding 3000 m and approaching 4000 m (Chase et al., 1998; DeCelles & Coogan, 2006; Sewall & Fricke, 2013; Foreman et al., 2015). We require catchment maximum relief and therefore set R=3,500–4,000 m (Table 2).

We also require constraints on paleoclimate; here, we used paleoclimate GCM results to estimate catchment-averaged paleoclimate (Figure 5c–e). HadCM3L is a coupled atmosphere–ocean GCM and is regularly implemented in deep-time paleoclimate studies (Tindall et al., 2010; Craggs et al., 2012; Lunt et al., 2016). HadCM3L has a spatial resolution of 2.5° latitude × 3.75° longitude and, relative to higher resolution GCMs, is fast and allows millennial to multi-millennial scale integrations (Farnsworth et al., 2019a). This is essential for paleoclimate modelling where initial boundary conditions are far from final equilibrium states. The HadCM3L results we used are identical to those presented in Farnsworth et al. (2019a), with atmospheric CO_2 prescribed as 1120 ppmv (×4 preindustrial atmospheric CO_2), and the exact model is similar to the HadCM3BLM2.1aD model described in Valdes et al. (2017). HadCM3L recovers mean annual and interannual paleoclimate variables. The mean annual climate variables we used were mean annual air temperature at 1.5 m above the local surface (Figure 5c) and mean annual precipitation (Figure 5d) and the interannual climate variable we used was mean precipitation of the wettest month in a simulated year (Figure 5e). Further details regarding the HadCM3L model and simulations used in this study are presented in the Supplement.

The Last Chance Ferron catchment was situated at ~45°paleolatitude (Bhattacharya & Tye, 2004; Bhattacharya et al., 2016), and we therefore used HadCM3L outputs at these paleolatitudes to assign reasonable bounds on catchment mean annual temperature, T, mean annual precipitation, P_{mean}, and mean precipitation of the wettest month in a simulated year, P_{peak}, for our analyses (Table 2).

ii.   Water discharges

We estimated Q_w as

$$Q_w = aPA$$ Eq. 7

where P is P_{mean} or P_{peak} and a is the runoff:rainfall ratio, which captures infiltration and evapotranspiration effects. When P_{mean} is used, Q_w reflects mean Q_w, whereas when P_{peak} is used, Q_w reflects mean Q_w of the wettest month. We initially assumed a=1, i.e., that all precipitated water enters streamflow, which recovers an estimate of maximum Q_w, and we later consider the implication of this assumption.

iii.   Sediment fluxes

We then estimated mean annual Q_s using the BQART model, an empirically derived model of long-term (>30 years) average suspended sediment flux (Syvitski & Milliman, 2007) which is increasingly used to reconstruct sediment fluxes in ancient systems (Allen et al., 2013; Lin & Bhattacharya, 2017; Watkins et al., 2018b; Zhang et al., 2018; Lyster et al., 2020). Using BQART, Q_s is approximated as

$$Q_s = \omega B Q_w^{0.31} A^{0.5} RT,$$ Eq. 8

where ω is a unit conversion constant (0.0006), Q_w is mean Q_w (i.e., derived using P_{mean}) and has units of km³/yr, A has units of km², R has units of km, and T has units of °C (Syvitski & Milliman, 2007). B is a glacial, lithologic, and anthropogenic factor which, for geological applications, we set to 1 (c.f. Lyster et al.,

2020). Equation 8 is for catchments in which T≥2°C. To implement Equation 8, we used previously outlined estimates of Q_w, A, R, and T (Table 2), which recovered estimates of Q_s in units of Mt/yr (1 Mt=10^9 kg), and which we converted to units of m³/yr assuming a plausible sediment porosity of 40% and sediment grain density of 2650 kg/m³ (c.f. Lyster et al., 2020).

4.3 Estimates of flow intermittency, I_w

i.   Approach 1

Approach 1 to estimate I_w combined field data and paleoclimate GCM results. We used field-derived estimates of channel-forming Q_w (i.e., $Q_{w(cf)}$), GCM-derived estimates of mean Q_w, and Equation 1 to estimate I_w. We did this twice; first, using estimates of channel-forming Q_w that we derived for dominant sand-transporting conditions and, second, using the larger estimates of channel-forming Q_w that we derived for gravel-transporting conditions.

ii.   Approach 2

Approach 2 to estimate I_w solely implemented paleoclimate GCM results. Here, we used GCM-derived estimates of the mean Q_w of the wettest month, GCM-derived estimates of the mean Q_w, and Equation 1 to estimate I_w. Estimates of mean Q_w were derived using mean precipitation (P_{mean}) and therefore reflect mean conditions (Equation 7). Meanwhile, estimates of mean Q_w during the wettest month were derived using mean precipitation of the wettest month (P_{peak}) (Equation 7). We suggest that estimates of mean Q_w during the wettest month potentially reflect the largest discharge conditions and, to implement Equation 1, we therefore used these estimates as a proxy for channel-forming Q_w. Specifically, we suggest that mean Q_w during the wettest month is a proxy for gravel-transporting channel-forming Q_w.

4.4 Estimates of sediment transport intermittency, I_s

i.   Approach 1

Our first approach to estimate I_s is based on stratigraphic observations. We used field-derived estimates of the channel-forming Q_s (i.e., $Q_{s(cf)}$), an estimate of the Last Chance Ferron depositional volume (i.e., $\sum Q_s$), and Equation 2 to calculate I_s. Channel-scale paleohydrologic methods to reconstruct sediment flux recover the total bed material load flux — they do not recover the total sediment flux including the entirely suspended fraction. Therefore, we specifically reconstructed the channel-forming bed material load ($Q_{bm(cf)}$), and we assumed the total depositional volume reflects $\sum Q_{bm}$. As channel-fill facies of the Last Chance Ferron Sandstone are dominated by sand-grade deposits, we focused on reconstructing I_s associated with sand-transporting conditions for these analyses.

The Last Chance Ferron depositional sequence stratigraphy has been mapped in detail along the dip section (i.e., proximal to distal; Figure 3) and, from this, we established this 2D dip-section area. We then assumed a 180° solid of revolution to estimate the 3D depositional volume (Figure 3, inset). This method involved a number of assumptions, and our estimate is therefore tentative. On one hand, we are overestimating the depositional volume because: (1) we used the entire 2D dip-section area and did not "remove" sediments that were not fluvially transported (i.e., coals) as this would be difficult to implement robustly at scale; (2) we assumed all sediments were transported as part of the bed material load, however it is possible that the finest fractions (perhaps in pro-delta and offshore facies) were transported in the entirely suspended fraction; (3) we did not remove pore space (~9% in shallow wells and ~4% in deep wells; Jarrard et al. (2004)) from the depositional volume to recover the grain volume. Therefore, we may consider this volume a maximum volume. Conversely, we are underestimating the depositional volume because we assumed zero erosion, which is unlikely. To address these uncertainties, we implemented a range of values that reflects our calculated value ±10%, therefore assigning a range for maximum depositional volume, or $\sum Q_{bm}$, of 430–530 km³ (Table 2).

Using estimates of $Q_{bm(cf)}$ and $\sum Q_{bm}$, we calculated the minimum time required to accumulate the observed stratigraphic thickness. Then, knowing the depositional timespan (i.e., t) of the Last Chance Ferron Sandstone was 1.7 million years, we calculated I_s using Equation 2.

ii.　　　Approach 2

Approach 2 to estimate I_s combined field data and paleoclimate GCM results. Here, we used field-derived estimates of channel-forming Q_{bm} (i.e., $Q_{bm(cf)}$), GCM-derived estimates of mean annual Q_s, which, when multiplied by the depositional timespan of the Last Chance Ferron Sandstone, reflects $\sum Q_s(t)$, and Equation 2 to estimate I_s. Importantly, field-derived estimates of $Q_{bm(cf)}$ are specific to bed material loads, whereas GCM-derived estimates of mean annual Q_s reflect suspended sediment loads. To make these constraints useful, we take estimates of $\sum Q_s(t)$ and estimate the theoretical $\sum Q_{bm}(t)$ using plausible bedload to suspended load ratios (Watkins et al., 2018a; Watkins, 2019). For large sand bed rivers, bedload to suspended load ratios are of order 0.01 to 0.05 (e.g., Cantalice et al., 2013; Sadeghi & Kheirfam, 2015; Lemma et al., 2019; Ashley et al., 2020; Namsai et al., 2020). We implemented an initial ratio of 0.05 and, using estimates of $Q_{bm(cf)}$ and theoretical $\sum Q_{bm}(t)$, we then estimated I_s using Equation 2. We later consider the sensitivity of our results to different bedload to suspended load ratios.

5. Results
5.1 Field results

Cross-sets were predominantly sand-grade, with a median D_{50} of 0.75 mm, a mean and standard deviation of D_{50} of 0.76 and 0.36 mm, respectively, and a minimum−maximum D_{50} of 0.38−3 mm (Figure 6a; Table 2). Meanwhile, for gravel-grade lenses and horizons, median D was 4 mm with a mean and standard deviation of 6.0 and 4.8 mm, respectively, and a minimum−maximum of 2−40 mm (Figure 6b; Table 2). For cross-sets, median h_{xs} was 0.14 m with a mean and standard deviation of 0.17 and 0.11 m, respectively, and a minimum−maximum of 0.01−0.64 m (Figure 6c; Table 2). Finally, measured flow depth proxies (including secondary data from literature) suggest median H is 5.6 m with a mean and standard deviation of 5.8 m and 3.0 m, respectively, and a minimum−maximum value of 1.1−12.2 m (Figure 6d; Table 2).

5.2 Water discharges and sediment fluxes in Last Chance Ferron rivers

Using field results, estimated channel geometries (see Table 2) and Equations 3–6, we estimated $Q_{w(cf)}$ and $Q_{bm(cf)}$ for sand-transporting and gravel-transporting conditions, respectively (Figure 7). As sand-grade deposits dominate channelized fluvial sandstone bodies, we assumed that sand-transporting flow conditions are the dominant channel-forming condition. For sand-transporting conditions, we estimated that $Q_{w(cf)}$ had a median value of ~2350 m³/s and an interquartile range of ~1760−2950 m³/s (Figure 7a), and that $Q_{bm(cf)}$ had a median value of ~0.22 m³/s and an interquartile range of ~0.15−0.30 m³/s (Figure 7b). Meanwhile for gravel-transporting flow conditions, which we assumed reflect the largest formative flow conditions, and which were infrequent in the preserved stratigraphy, we estimated that $Q_{w(cf)}$ had a median value of ~4900 m³/s and an interquartile range of ~4310−5560 m³/s (Figure 7c), and that $Q_{bm(cf)}$ had a median value of ~26.6 m³/s and an interquartile range of ~23.2−30.5 m³/s (Figure 7d).

Using GCM results and Equations 7 and 8, we calculated mean Q_w and mean Q_w during the wettest month (Figure 8). For mean Q_w, we estimated a median value of ~1620 m³/s and an interquartile range of ~1480−1750 m³/s (Figure 8a). For mean Q_w during the wettest month, we estimated a median value of ~7130 m³/s and an interquartile range of ~6530−7720 m³/s (Figure 8c). To facilitate comparison between instantaneous and mean conditions, we present results in units of both m³/s and m³/yr in Figure 8a–d. Also, we remind the reader that we assumed $a=1$ in Equation 7, and we highlight that implementing $a<1$ acts to lower estimates of mean Q_w and mean Q_w during the wettest month.

Finally, we used GCM results and Equations 7 and 8 to estimate mean annual Q_s, and we estimated a median value of 1.43×10^7 m³/yr and an interquartile range of 1.26×10^7–1.61×10^7 m³/yr (Figure 8e). Similarly, we present results in units of both m³/s and m³/yr in Figure 8e,f.

5.3 Flow intermittency in Last Chance Ferron rivers

Using Approach 1, based on field constraints and GCM results, estimates of sand-transporting I_w had a median value of 0.68 and an interquartile range of 0.54−0.90 (Figure 9a). Here, median I_w is equivalent to 248 days (or ~8 months) per year, and the interquartile range is equivalent to 197−329 days (or ~6.4–10.6 months) per year. Estimates of gravel-transporting I_w had a median value of 0.33 and an interquartile range of 0.28−0.38 (Figure 9a). Here, median I_w is equivalent to 120 days (or ~4 months) per year, and the interquartile range is equivalent to 102−139 days (or ~3.3–4.5 months) per year. Meanwhile, using Approach 2, based on GCM results alone, estimates of I_w had a median value of 0.23 and an interquartile range of 0.21−0.25 (Figure 9a). Here, median I_w is equivalent to 84 days (just under 3 months) per year, and the interquartile range is equivalent to 77−91 days (or ~2.5–3 months) per year.

In comparing Approach 1 and 2, we highlight that I_w values derived from Approach 1 for gravel-transporting conditions are most similar to, but still larger than, I_w values derived from Approach 2 (Figure 9a). Importantly, Approach 2 used GCM results alone and, therefore, implementing $a<1$ in Equation 7 does not change the implied I_w values (Equation 1). However, for Approach 1, implementing $a<1$ in Equation 7 acts to decrease the implied I_w values. Depending on the assumed value of a, this will make I_w values derived from Approach 1 for gravel-transporting conditions smaller and, therefore, more similar to those derived from Approach 2 (Figure 9a). In detail, these values would coincide if we assumed a plausible value for a of 0.6–0.7.

5.4 Sediment transport intermittency in Last Chance Ferron rivers

Using Approach 1, our estimates of I_s had a median value of 0.040 and an interquartile range of 0.028−0.057 (Figure 9b). Here, median I_s is equivalent to ~15 days per year, and the interquartile range is equivalent to 10−21 days per year. Meanwhile, using Approach 2, estimates of I_s had a median value of 0.11 and an interquartile range of 0.075−0.15 (Figure 9b). Here, median I_s is equivalent to ~40 days per year, and the interquartile range is equivalent to 27−55 days per year. Estimates of I_s derived from Approach 2 were a factor of ~2−3 larger than estimates derived from Approach 1 (Figure 9b). In Approach 2 we assumed a bedload to suspended load ratio of 0.05, and we highlight that decreasing this ratio (to 0.01, perhaps) acts to decrease the implied I_s (Figure 9b). At this point we highlight that I_s values are significantly smaller than I_w values, and we return to this in the discussion.

6. Discussion
6.1 Implications of intermittency estimates for Last Chance Ferron rivers

Constraints on I_w and I_s reflect the time-dependent integral of the river hydrograph, and therefore provide a baseline from which we can probe the temporal distribution of flow and sediment transport in the geological past. For a given I_w, there are a range of possible hydrograph scenarios (Figure 1a–d) and, likewise, for a given I_s, there are a range of possible "sediment graph" scenarios (Figure 1e–h). Importantly, the temporal distributions of flow and sediment transport are not necessarily correlated. For flashy ephemeral rivers, we might expect I_w and I_s to converge, given the increased likelihood of all sediment transport occurring during channel-forming conditions. Meanwhile, for perennial rivers, we might expect I_w and I_s to diverge, with I_s values lower than I_w values, given the likelihood of regular moderate (i.e., non-channel forming) flow taking place in which limited sediment transport might be expected.

For Last Chance Ferron rivers we estimated sand-transporting I_w values of 0.54−0.90 which, assuming sand-transporting conditions were the dominant channel-forming condition, suggests that annual water

budgets could have been transported in ~6.4–10.6 months of the year if channel-forming conditions were sustained (Figure 9a). Channel-forming conditions are often attributed to bankfull flow stages, but this is not necessarily the case given the typical durations and recurrence intervals of bankfull conditions (Wolman & Miller, 1960; Woodyer, 1968; Dunne & Leopold, 1978; Williams, 1978), and given the potential for the fluvial stratigraphic record to preserve ordinary flow conditions (Ganti et al., 2014; Paola et al., 2018; Ganti et al., 2020; Holbrook & Miall, 2020). Considering potential hydrograph scenarios (Figure 1a–d), sand-transporting $Q_{w(cf)}$ values of ~1760−2950 m³/s and I_w values of 0.54−0.90 suggest that channel-forming discharges persisted for the majority of the year. In Figure 9a, the whisker of the sand-transporting $I_{f(w)}$ boxplot extends to 1, which suggests that channel-forming discharges were potentially sustained all year around. These results are consistent with ever-wet perennial systems in which relatively high discharges are sustained, as opposed to perennial systems in which discharge is sustained but there is a characteristic seasonal low discharge (relative to the mean discharge).

In contrast, we estimated gravel-transporting I_w values of 0.28−0.38 which, assuming gravel-transporting conditions were not the dominant channel-forming condition, but potentially reflect the largest formative flow conditions, suggests that the largest discharge events may have occupied Last Chance Ferron rivers for ~3.3–4.5 months of the year (Figure 9a). One explanation for this is that the largest discharge events (~4310−5560 m³/s) were sustained events, such as in monsoonal climates where flood durations are of order weeks to months (Serinaldi et al., 2018). An alternative explanation is that stochastic weather events, such as subtropical storms, generated high magnitude discharge events that were shorter in duration, but which had sufficiently high frequencies to occupy one third of the year. In Approach 2, we used GCM estimates of the mean precipitation of the wettest month, and their derivative water discharge estimates, as proxies for the largest formative flow conditions. In turn, GCM-derived estimates of I_w suggest that the largest discharge events (~6530−7720 m³/s) may have been sustained for ~2.5–3 months of the year (Figure 9a). There is broad agreement between GCM-derived estimates of mean Q_w during the wettest month and field-derived estimates of gravel-transporting $Q_{w(cf)}$, especially if we consider that implementing $a<1$ in Equation 7 acts to reduce estimates of mean Q_w during the wettest month (Figures 7,8). In detail, implementing plausible values for a of 0.6–0.7 would reduce these values sufficiently to reach agreement. This suggests that GCM estimates of the mean precipitation of the wettest month may provide reasonable proxies for the largest formative flow events and, therefore, a potentially useful method to estimate flow intermittency factors of the largest discharge events in the geological past.

The introduction of sediment transport intermittency factors was primarily motivated by the need to upscale estimates of instantaneous Q_s to mean annual Q_s in geological investigations of basin evolution and, in doing so, the value of I_s is typically an assumed value (Paola et al., 1992). Here, however, we actively estimated I_s using estimates of both instantaneous Q_s and mean annual Q_s, and we can use our estimated I_s values to probe the effect of climate change on sediment budgets in Last Chance Ferron rivers. As channelized fluvial sandstones were dominated by sand-grade deposits, we focused on calculating I_s values associated with sand-transporting conditions. Using Approach 1, we estimated I_s values of 0.028−0.057 which, assuming that channel-forming conditions do all geomorphic work, suggests that annual sediment budgets could have been transported in as little as 10−21 days per year if channel-forming conditions were sustained (Figure 9b). Using Approach 2, we estimated I_s values of 0.075−0.15 which suggests that annual sediment budgets could have been transported in 27−55 days per year if channel-forming conditions were sustained (Figure 9b). For reference, estimated I_s values in modern rivers include I_s values of ~0.3−0.34 for the Mississippi River, USA (Wright & Parker, 2005), and I_s values of 0.175 for one of the Mississippi River's tributaries, the Minnesota River (Czuba & Foufoula-Georgiou, 2014).

If 10−21 days of channel-forming flow could do all mass-transport work in Last Chance Ferron rivers, then an additional few days of channel-forming flow would be sufficient to significantly increase the sediment budget in any one year. In monsoonal rivers this could be achieved by an extended monsoonal wet season,

whereas in subtropical or perennial rivers this could be achieved by a few extra storm events per year. Using Approach 2, if 27−55 days of channel-forming flow could do all geomorphic work, then a much larger increase in the duration of channel-forming flows would be required to significantly increase annual sediment budgets.

6.2 Independent insights into intermittency

With multiple possible hydrograph scenarios, we can use independent insights into flow intermittency from facies-based observations of seasonal–interannual flow variability, terrestrial paleoclimate studies, and more to identify the most plausible hydrograph scenario (Figure 1).

In the Late Cretaceous Western Interior, GCMs generally predict that a strong monsoon prevailed along the eastern flank of the Sevier mountains (western North American landmass; Figure 2b inset) (Fricke et al., 2010; Foreman et al., 2011; Sewall & Fricke, 2013). This prediction is corroborated by oxygen isotope data from bivalve shells and paleosol carbonates, which indicate an east–west movement of water vapour from low elevations (WIS) to high elevations (Sevier mountains) and point to the recharge of rivers in the Sevier foreland by high elevation precipitation (Fricke et al., 2010). This would suggest hydrographs characterized by sustained flood events, as opposed to hydrographs characterized by multiple short-lived flood events or persistent high discharge (Figure 1a–d). In the case of Last Chance Ferron rivers, our estimates of I_w might manifest as hydrographs characterized by sustained flood events during the monsoonal wet season, with peak discharges of order 5000 m³/s (Figures 7c), perhaps up to ~7000 m³/s (Figure 8b), and by relatively high discharges throughout the monsoonal dry season, with channel-forming discharges of order 2000 m³/s (Figure 7a).

While floodplain facies have not been analysed for the Last Chance Ferron fluvial-deltaic complex, detailed analyses of floodplain facies in the neighbouring Notom Ferron fluvial-deltaic complex also point to a paleoclimate characterized by sustained wet periods (Famubode, 2014; Akyuz et al., 2015; Famubode & Bhattacharya, 2016). In the Notom Ferron Sandstone, palynological analysis has recognized a predominance of moisture-loving terrestrial palynomorphs that suggest deposition occurred in ever-wet subtropical–tropical environments (Akyuz et al., 2015), and the presence of hydromorphic paleosols, or "gleysols" (Mack et al., 1993) indicate conditions of soil saturation and waterlogging in poorly-draining floodplains (Famubode, 2014; Akyuz et al., 2015; Famubode & Bhattacharya, 2016). These hydromorphic paleosols are consistent with a persistent shallow water table, but infrequent presence of weak to well-developed pedogenic structures and shrink-and-swell structures suggests periodic drying associated with episodic water table lowering (Famubode, 2014). Here, interpretation of a fluctuating water table has been attributed to fluctuating wet and dry periods which, in turn, has been attributed to a paleoclimate characterized by low seasonality, in which wet months exceeded dry months (Famubode, 2014).

For the Last Chance Ferron Sandstone, we also note the presence of hydromorphic paleosols in floodplain deposits, distinguishable by their dull grey low-chroma colours (Figure 4b), which is consistent with the neighbouring Notom fluvio-deltaic complex and supports interpretation of sustained wet periods. More distally, the abundance of organic matter and coals throughout the Last Chance Ferron fluvial-deltaic complex (Cotter, 1976; Garrison Jr et al., 1997; Garrison Jr & van den Bergh, 2004), also suggests poorly drained and reducing conditions and corroborates interpretation of sustained wet periods.

While independent insights generally point to ever-wet perennial systems in which the largest discharge events were sustained (e.g., Figure 1c,d), further work is required to identify the causes of the largest discharge events. Recent work on the Last Chance Ferron Sandstone documented abundant evidence for bedform disequilibrium dynamics, which may provide insights into formative flow durations (Lyster et al., 2022b). Assuming that bedform disequilibrium dynamics reflect near-instantaneous flow variability, Lyster et al. (2022b) estimated total flood durations of order a few hours to a few days, consistent with floods

caused by heavy rains, torrential storms, and sub-tropical or extra-tropical storms, which are typical of perennial systems. In this scenario, sand-transporting and gravel-transporting I_w values of 0.54−0.90 and 0.28−0.38, respectively, would necessitate high frequencies of these short-duration flood events, which is at odds with observations that point to more sustained flood events. Both scenarios are consistent with the abundance of thin, sparsely bioturbated, waning-flow sandstone beds and diffusely laminated mudstones on the Last Chance Ferron delta front, which are interpreted respectively as hyperpycnal flows and associated fluid muds generated by river floods (Bhattacharya & MacEachern, 2009).

Overall, independent insights into seasonal–interannual flow variability enable us to contextualise our estimated I_w values and begin to probe how flow was distributed in time, i.e., the shape of river hydrographs (Figure 1a–d). However, further work is required to refine these insights.

6.3 Estimating intermittency in the geological past: future directions

We show that paleoclimate GCMs present new opportunities to estimate water discharges and sediment fluxes in ancient catchments and, therefore, constrain intermittency factors in the geological past.

We presented two methods to estimate I_w values, both of which implemented paleoclimate GCM results. One is a combined stratigraphic–paleoclimate GCM approach, and the other is a paleoclimate GCM approach. With continual advances in the use of GCMs to model paleoclimates (e.g., Lunt et al., 2016; Tabor et al., 2016; Farnsworth et al., 2019a), including extreme paleoclimates, e.g., monsoons (Abe et al., 2003; Fricke et al., 2010; Kitoh et al., 2010; Marzocchi et al., 2015; Farnsworth et al., 2019b), our results highlight the potential to use paleoclimate GCMs to constrain intermittency in the geological past, particularly where the rock record is incomplete or inaccessible. These opportunities are also applicable to planetary examples, given interest in deciphering timespans of fluvial activity on Mars (Moore et al., 2003; Jerolmack et al., 2004; Kleinhans, 2005; Buhler et al., 2014; Stucky de Quay et al., 2019; Lapôtre & Ielpi, 2020; Hayden et al., 2021a) and ongoing efforts to model early Mars paleoclimate (Wordsworth et al., 2015; Wordsworth, 2016; Steakley et al., 2019; Kamada et al., 2020; Ramirez et al., 2020; Guzewich et al., 2021).

In addition, we presented two methods to estimate I_s values — a stratigraphic approach and a combined stratigraphic–paleoclimate GCM approach. Our results demonstrate that paleoclimate GCMs will be particularly useful to estimate I_s where stratigraphic approaches are challenging to implement. Stratigraphic approaches to estimate I_s require mass balance assumptions, which are feasible in trunk channels of single-thread rivers and apex feeder channels in fluvial fans, however in multi-thread systems and fluvial fans they require knowledge of the number of active threads (including thread widths). Further, mass balance assumptions inherently require good constraints on preserved depositional volumes, which can be challenging (especially for depositional systems in open basins, in which there may be significant net-import or net-export of sediment mass). Using paleoclimate GCM results evades the need for mass balance assumptions and well-constrained depositional volumes.

Going forward, our ability to constrain intermittency in the geological past will benefit from continued advances to paleoclimate GCMs but, more importantly, from development of useful methods to apply paleoclimate GCM results to geological questions. I_s values are often documented in modern systems (e.g., Meybeck et al., 2003; Sklar & Dietrich, 2004; Wright & Parker, 2005; Czuba & Foufoula-Georgiou, 2014; Hayden et al., 2021a), which facilitates comparison between modern and ancient systems (e.g., Hayden et al., 2021a; Hayden et al., 2021b). However, I_w values are typically not documented in modern systems. Instead, research communities tend to document various seasonal–interannual flow variability metrics in modern systems, such as average discharge variability indexes, discharge peakedness, cumulative discharge variability indexes, and more (see review by Hansford et al., 2020). While these metrics are readily measurable in modern systems, implementing them in geological investigations is non-trivial because they require information that cannot always be determined.

Currently, geological investigations of seasonal–interannual flow variability and, by proxy, flow intermittency are limited to qualitative descriptions of discharge regime from fluvial strata (e.g., Fielding et al., 2009; Plink-Björklund, 2015). Here, we showed that paleoclimate GCMs can be used to quantify flow intermittency and, by proxy, seasonal–interannual flow variability. Further, the paleoclimate GCM results that we used to achieve this included mean annual precipitation and mean precipitation of the wettest month. In using these climate variables to estimate flow intermittency (Equation 1), we effectively estimated the inverse of discharge peakedness, which is defined as the ratio of the mean discharge during the month with the highest discharge to the mean discharge (Hansford et al., 2020). Not only have we highlighted the potential to use paleoclimate GCMs to quantitatively explore flow intermittency and, by proxy, seasonal–interannual flow variability in the geological past, but we have also shown that paleoclimate GCMs can be used to derive metrics, such as discharge peakedness, for ancient systems that are more readily comparable with modern systems in which these metrics are routinely documented (Hansford et al., 2020).

7. Conclusion

Intermittency factors describe the fraction of time in which constant channel-forming conditions could transport the same amount of water or sediment as the actual hydrograph does. They are an important, but underutilized, metric to probe the temporal distribution of flow and sediment transport in the geological past. We demonstrate for the first time how we can combine stratigraphic field data, flow and sediment transport models, and paleoclimate GCM results to constrain flow and sediment transport intermittency in the geological past. In detail, intermittency factors reflect the time-dependent integral of the river hydrograph, and we show how these constraints can be used, in conjunction with independent facies-based and proxy-based insights, to probe hydrograph shapes in ancient rivers.

We demonstrate our methods for the Upper Cretaceous Last Chance Ferron Sandstone, Utah, USA. For Last Chance Ferron rivers, we estimate sand-transporting flow intermittency factors of 0.54−0.90, which suggest that channel-forming conditions were sustained all year around. These results point to a perennial system in which high discharge was sustained, as opposed to a perennial system in which there was a characteristic seasonal low discharge. In addition, gravel-transporting flow intermittency factors of 0.28−0.38 suggest that the largest formative flows may have occupied Last Chance Ferron rivers for nearly a third of the year. One explanation is that the largest formative flows were sustained events, such as in monsoonal climates where flood durations are of order weeks to months, whereas an alternative explanation is that subtropical climates prevailed in which storm events were shorter in duration but higher in frequency. Meanwhile, sediment transport intermittency factors as small as 0.028−0.057, but up to 0.075−0.15, suggest that entire sediment budgets could have been delivered in as little as 10 days of the year, but up to 2 months. These insights highlight the potential impact of slight increases in the magnitude and/or frequencies of channel-forming flow conditions on total sediment budgets. Independent insights into seasonal– interannual flow variability for the Last Chance Ferron system corroborate interpretation of ever-wet systems in which the largest formative flows are sustained, which helps to narrow down potential hydrograph shapes. However, further work is required to identify the causes of the largest formative flows and therefore refine hydrograph shapes.

Our results help to close the gap between instantaneous and mean timescales of investigation, and they provide new insights into the transport of water and mass across Earth's surface in the geological past. We highlight that paleoclimate GCMs will be particularly useful to investigate intermittency where the rock record is incomplete or inaccessible, or where stratigraphic approaches are limited. Going forward, we suggest that paleoclimate GCMs will enable us to tackle pertinent research questions concerning past surface processes on both Earth and other terrestrial planetary bodies.

Author contributions

SJL and ACW designed the study and conducted field data collection, with guidance from GJH. SJL processed field data and results. AF performed paleoclimate model simulations. SJL, ACW and GJH analysed and interpreted results. SJL wrote the manuscript. ACW, AF, and GJH all contributed significantly to the manuscript.

Data Availability

Field data are available are in the supplementary material.

References

Abe, M., Kitoh, A., & Yasunari, T. (2003). An evolution of the Asian Summer Monsoon associated with mountain uplift; Simulation with the MRI Atmosphere-Ocean Coupled GCM. *Journal of the Meteorological Society of Japan. Ser. II*, *81*(5), 909-933. DOI:10.2151/jmsj.81.909

Akyuz, I., Warny, S., Famubode, O., & Bhattacharya, J. (2015). Palynology of the Upper Cretaceous (Turonian) Ferron Sandstone Member, Utah, USA: Identification of marine flooding surfaces and Milankovitch cycles in subtropical, ever-wet, paralic to non-marine palaeoenvironments. *Palynology*, *40*. DOI:10.1080/01916122.2015.1014525

Allen, P. A., Armitage, J. J., Carter, A., Duller, R. A., Michael, N. A., Sinclair, H. D., Whitchurch, A. L., & Whittaker, A. C. (2013). The Q_s problem: Sediment volumetric balance of proximal foreland basin systems. *Sedimentology*, *60*(1), 102-130. DOI:10.1111/sed.12015

Anderson, P. B., & Ryer, T. A. (2004). Regional Stratigraphy of the Ferron Sandstone. In T. C. Chidsey, Jr., R. D. Adams, & T. H. Morris (Eds.), *Regional to Wellbore Analog for Fluvial-Deltaic Reservoir Modeling: The Ferron Sandstone of Utah* (Vol. 50, pp. 0). American Association of Petroleum Geologists. https://doi.org/10.1306/St50983

Ashley, T. C., McElroy, B., Buscombe, D., Grams, P. E., & Kaplinski, M. (2020). Estimating Bedload From Suspended Load and Water Discharge in Sand Bed Rivers. *Water Resources Research*, *56*(2), e2019WR025883. DOI:10.1029/2019WR025883

Bestland, E. A., Retallack, G. J., & Swisher Iii, C. C. (1997). Stepwise Climate Change Recorded in Eocene-Oligocene Paleosol Sequences from Central Oregon. *The Journal of Geology*, *105*(2), 153-172. DOI:10.1086/515906

Bhattacharya, J. P., Copeland, P., Lawton, T. F., & Holbrook, J. (2016). Estimation of source area, river paleo-discharge, paleoslope, and sediment budgets of linked deep-time depositional systems and implications for hydrocarbon potential. *Earth-Science Reviews*, *153*, 77-110. DOI:10.1016/j.earscirev.2015.10.013

Bhattacharya, J. P., Payenberg, T. H. D., Lang, S. C., & Bourke, M. (2005). Dynamic river channels suggest a long-lived Noachian crater lake on Mars. *Geophysical Research Letters*, *32*(10). DOI:10.1029/2005GL022747

Bhattacharya, J. P., & Tye, R. S. (2004). Searching for Modern Ferron Analogs and Application to Subsurface Interpretation. In T. C. Chidsey, Jr., R. D. Adams, & T. H. Morris (Eds.), *Regional to Wellbore Analog for Fluvial-Deltaic Reservoir Modeling: The Ferron Sandstone of Utah* (Vol. 50, pp. 0). American Association of Petroleum Geologists. https://doi.org/10.1306/St50983

Bhattacharyya, P., Bhattacharya, J. P., & Khan, S. D. (2015). Paleo-channel reconstruction and grain size variability in fluvial deposits, Ferron Sandstone, Notom Delta, Hanksville, Utah. *Sedimentary Geology*, *325*, 17-25. DOI:10.1016/j.sedgeo.2015.05.001

Birgenheier, L. P., Berg, M. D. V., Plink-Björklund, P., Gall, R. D., Rosencrans, E., Rosenberg, M. J., Toms, L. C., & Morris, J. (2019). Climate impact on fluvial-lake system evolution, Eocene Green River Formation, Uinta Basin, Utah, USA. *GSA Bulletin*, *132*(3-4), 562-587. DOI:10.1130/B31808.1

Buhler, P. B., Fassett, C. I., Head, J. W., & Lamb, M. P. (2014). Timescales of fluvial activity and intermittency in Milna Crater, Mars. *Icarus, 241*, 130-147. DOI:10.1016/j.icarus.2014.06.028

Cantalice, J. R. B., Cunha Filho, M., Stosic, B. D., Piscoya, V. C., Guerra, S. M. S., & Singh, V. P. (2013). Relationship between bedload and suspended sediment in the sand-bed Exu River, in the semi-arid region of Brazil. *Hydrological Sciences Journal, 58*(8), 1789-1802. DOI:10.1080/02626667.2013.839875

Chase, C. G., Gregory-Wodzicki, K. M., Parrish, J. T., & DeCelles, P. G. (1998). Topographic history of the Western Cordillera of North America and controls on climate. In T. J. Crowley & K. Burke (Eds.), *Tectonic Boundary Conditions for Climate Reconstructions* (Vol. 39, pp. 73-99). Oxford Monographs on Geology and Geophysics.

Chen, C., Guerit, L., Foreman, B. Z., Hassenruck-Gudipati, H. J., Adatte, T., Honegger, L., Perret, M., Sluijs, A., & Castelltort, S. (2018). Estimating regional flood discharge during Palaeocene-Eocene global warming. *Scientific Reports, 8*(1), 13391. DOI:10.1038/s41598-018-31076-3

Chidsey, T. C., Adams, R. D., & Morris, T. H. (2004). *Regional to Wellbore Analog for Fluvial-Deltaic Reservoir Modeling: The Ferron Sandstone of Utah* (Vol. 50). https://doi.org/10.1306/St50983

Clark, C., II, Nnaji, G. A., & Huang, W. (2014). Effects of El-Niño and La-Niña Sea Surface Temperature Anomalies on Annual Precipitations and Streamflow Discharges in Southeastern United States. *Journal of Coastal Research*(68 (10068)), 113-120. DOI:10.2112/SI68-015.1

Cotter, E. (1971). Paleoflow characteristics of a late Cretaceous river in Utah from analysis of sedimentary structures in the Ferron sandstone. *Journal of Sedimentary Research 41*, 129–138. DOI:10.1306/74D72202-2B21-11D7-8648000102C1865D

Cotter, E. (1975a). Deltaic deposits in the Upper Cretaceous Ferron Sandstone, Utah. In M. L. Broussard (Ed.), *Deltas: Models for Exploration* (pp. 471-484). Houston Geological Society.

Cotter, E. (1975b). Late Cretaceous sedimentation in a low-energy coastal zone; the Ferron Sandstone of Utah. *Journal of Sedimentary Research, 45*(3), 669-685. DOI:10.1306/212F6E0B-2B24-11D7-8648000102C1865D

Cotter, E. (1976). The role of deltas in the evolution of the Ferron Sandstone and its coals. *Brigham Young University Geology Studies, 22*, 15-41.

Craggs, H. J., Valdes, P. J., & Widdowson, M. (2012). Climate model predictions for the latest Cretaceous: An evaluation using climatically sensitive sediments as proxy indicators. *Palaeogeography, Palaeoclimatology, Palaeoecology, 315-316*(Supplement C), 12-23. DOI:10.1016/j.palaeo.2011.11.004

Czuba, J. A., & Foufoula-Georgiou, E. (2014). A network-based framework for identifying potential synchronizations and amplifications of sediment delivery in river basins. *Water Resources Research, 50*(5), 3826-3851. DOI:10.1002/2013WR014227

Das, T., Maurer, E. P., Pierce, D. W., Dettinger, M. D., & Cayan, D. R. (2013). Increases in flood magnitudes in California under warming climates. *Journal of Hydrology, 501*, 101-110. DOI:10.1016/j.jhydrol.2013.07.042

DeCelles, P. G. (2004). Late Jurassic to Eocene evolution of the Cordilleran thrust belt and foreland basin system, western U.S.A. *American Journal of Science, 304*. DOI:10.2475/ajs.304.2.105

DeCelles, P. G., & Coogan, J. C. (2006). Regional structure and kinematic history of the Sevier fold-and-thrust belt, central Utah. *GSA Bulletin, 118*(7/8), 841-864. DOI:10.1130/B25759.1

Dunne, T., & Leopold, L. B. (1978). *Water in Environmental Planning*. W. H. Freeman.

Engelund, F., & Hansen, E. (1967). *A Monograph on Sediment Transport in Alluvial Streams*. Technisk Vorlag.

Famubode, O. A. (2014). *Paleosol evolution in a sequence stratigraphic framework, Cretaceous Ferron Notom Delta, south central Utah, U.S.A.* University of Houston].

Famubode, O. A., & Bhattacharya, J. P. (2016). Sequence Stratigraphic Analysis of the Youngest Nonmarine Sequence In the Cretaceous Ferron Notom Delta, South Central Utah, U.S.A. *Journal of Sedimentary Research, 86*(3), 168-198. DOI:10.2110/jsr.2016.8

Farnsworth, A., Lunt, D. J., O'Brien, C., Foster, G. L., Inglis, G. N., Markwick, P., Pancost, R. D., & Robinson, S. A. (2019a). Climate sensitivity on geological timescales controlled by non-linear feedbacks and ocean circulation. *Geophysical Research Letters, 0*(ja). DOI:10.1029/2019GL083574

Farnsworth, A., Lunt, D. J., Robinson, S. A., Valdes, P. J., Roberts, W. H. G., Clift, P. D., Markwick, P., Su, T., Wrobel, N., Bragg, F., Kelland, S.-J., & Pancost, R. D. (2019b). Past East Asian monsoon evolution controlled by paleogeography, not CO_2. *Science Advances, 5*(10), eaax1697. DOI:10.1126/sciadv.aax1697

Fernandes, V. M., Roberts, G. G., White, N., & Whittaker, A. C. (2019). Continental-Scale Landscape Evolution: A History of North American Topography. *Journal of Geophysical Research: Earth Surface, 124*(11), 2689-2722. DOI:10.1029/2018JF004979

Fielding, C. R. (2010). Planform and Facies Variability in Asymmetric Deltas: Facies Analysis and Depositional Architecture of the Turonian Ferron Sandstone in the Western Henry Mountains, South-Central Utah, U.S.A. *Journal of Sedimentary Research*, *80*(5), 455-479. DOI:10.2110/jsr.2010.047

Fielding, C. R., Alexander, J., & Allen, J. P. (2018). The role of discharge variability in the formation and preservation of alluvial sediment bodies. *Sedimentary Geology*, *365*, 1-20. DOI:10.1016/j.sedgeo.2017.12.022

Fielding, C. R., Allen, J. P., Alexander, J., & Gibling, M. R. (2009). Facies model for fluvial systems in the seasonal tropics and subtropics. *Geology*, *37*(7), 623-626. DOI:10.1130/G25727A.1

Foreman, B. Z., Fricke, H. C., Lohmann, K. C., & Rogers, R. R. (2011). RECONSTRUCTING PALEOCATCHMENTS BY INTEGRATING STABLE ISOTOPE RECORDS, SEDIMENTOLOGY, AND TAPHONOMY: A LATE CRETACEOUS CASE STUDY (MONTANA, UNITED STATES)Reconstructing Paleocatchments. *PALAIOS*, *26*(9), 545-554. DOI:10.2110/palo.2010.p10-133r

Foreman, B. Z., Heller, P. L., & Clementz, M. T. (2012). Fluvial response to abrupt global warming at the Palaeocene/Eocene boundary. *Nature*, *491*, 92-95. DOI:10.1038/nature11513

Foreman, B. Z., Roberts, E. M., Tapanila, L., Ratigan, D., & Sullivan, P. (2015). Stable isotopic insights into paleoclimatic conditions and alluvial depositional processes in the Kaiparowits Formation (Campanian, south-central Utah, U.S.A.). *Cretaceous Research*, *56*, 180-192. DOI:10.1016/j.cretres.2015.05.001

Fricke, H. C., Foreman, B. Z., & Sewall, J. O. (2010). Integrated climate model-oxygen isotope evidence for a North American monsoon during the Late Cretaceous. *Earth and Planetary Science Letters*, *289*(1-2), 11-21. DOI:10.1016/j.epsl.2009.10.018

Gaál, L., Szolgay, J., Kohnová, S., Hlavčová, K., Parajka, J., Viglione, A., Merz, R., & Blöschl, G. (2015). Dependence between flood peaks and volumes: a case study on climate and hydrological controls. *Hydrological Sciences Journal*, *60*(6), 968-984. DOI:10.1080/02626667.2014.951361

Gall, R. D., Birgenheier, L. P., & Berg, M. D. V. (2017). Highly seasonal and perennial fluvial facies: Implications for climatic control on the Douglas Creek and Parachute Creek members, Green River Formation, southeastern Uinta Basin, Utah, U.S.A. *Journal of Sedimentary Research*, *87*(9), 1019-1047. DOI:10.2110/jsr.2017.54

Ganti, V., Hajek, E. A., Leary, K., Straub, K. M., & Paola, C. (2020). Morphodynamic hierarchy and the fabric of the sedimentary record. *Geophysical Research Letters*, *47*(14), e2020GL087921. DOI:10.1029/2020GL087921

Ganti, V., Lamb, M. P., & McElroy, B. (2014). Quantitative bounds on morphodynamics and implications for reading the sedimentary record. *Nature Communications*, *5*(1), 3298. DOI:10.1038/ncomms4298

Ganti, V., Whittaker, A., Lamb, M. P., & Fischer, W. W. (2019). Low-gradient, single-threaded rivers prior to greening of the continents. *Proceedings of the National Academy of Sciences*, *116*(4), 11652-11657. DOI:10.1073/pnas.1901642116

García, M., & Parker, G. (1991). Entrainment of Bed Sediment Into Suspension. *Journal of Hydraulic Engineering-asce - J HYDRAUL ENG-ASCE*, *117*. DOI:10.1061/(ASCE)0733-9429(1991)117:4(414)

Gardner, M. H. (1995). Tectonic and Eustatic Controls on the Stratal Architecture of Mid-Cretaceous Stratigraphic Sequences, Central Western Interior Foreland Basin of North America. In S. L. Dorobek & G. M. Ross (Eds.), *Stratigraphic Evolution of Foreland Basins* (Vol. 52, pp. 0). SEPM Society for Sedimentary Geology. https://doi.org/10.2110/pec.95.52.0243

Gardner, M. H., Cross, T. A., & Levorsen, M. (2004). Stacking Patterns, Sediment Volume Partitioning, and Facies Differentiation in Shallow-Marine and Coastal-Plain Strata of the Cretaceous Ferron Sandstone, Utah. In T. C. Chidsey, Jr., R. D. Adams, & T. H. Morris (Eds.), *Regional to Wellbore Analog for Fluvial-Deltaic Reservoir Modeling: The Ferron Sandstone of Utah* (Vol. 50, pp. 0). American Association of Petroleum Geologists. https://doi.org/10.1306/St50983

Garrison Jr, J. R., & van den Bergh, T. C. V. (2004). High-Resolution Depositional Sequence Stratigraphy of the Upper Ferron Sandstone Last Chance Delta: An Application of Coal-Zone Stratigraphy. In T. C. Chidsey, Jr., R. D. Adams, & T. H. Morris (Eds.), *Regional to Wellbore Analog for Fluvial-Deltaic Reservoir Modeling: The Ferron Sandstone of Utah* (Vol. 50, pp. 0). American Association of Petroleum Geologists. https://doi.org/10.1306/St50983

Garrison Jr, J. R., van den Bergh, T. C. V., Barker, C. E., & Tabet, D. E. (1997). Depositional sequence stratigraphy and architecture of the Cretaceous Ferron Sandstone: Implications for coal and coalbed methane resources - a field excursion. In P. K. Link & B. J. Kowallis (Eds.), *Mesozoic to Recent geology of Utah, Brigham Young University Geology Studies* (Vol. 42, pp. 155-202). http://pubs.er.usgs.gov/publication/70019477

Goñi, M. A., Hatten, J. A., Wheatcroft, R. A., & Borgeld, J. C. (2013). Particulate organic matter export by two contrasting small mountainous rivers from the Pacific Northwest, U.S.A. *Journal of Geophysical Research: Biogeosciences*, *118*(1), 112-134. DOI:10.1002/jgrg.20024

Greenberg, E., Ganti, V., & Hajek, E. (2021). Quantifying bankfull flow width using preserved bar clinoforms from fluvial strata. *Geology*, *49*(9), 1038-1043. DOI:10.1130/G48729.1

Guzewich, S. D., Way, M. J., Aleinov, I., Wolf, E. T., Del Genio, A., Wordsworth, R., & Tsigaridis, K. (2021). 3D Simulations of the Early Martian Hydrological Cycle Mediated by a H2-CO2 Greenhouse. *Journal of Geophysical Research: Planets*, *126*(7), e2021JE006825. DOI:10.1029/2021JE006825

Hajek, E. A., & Heller, P. L. (2012). Flow-depth scaling in alluvial architecture and nonmarine sequence stratigraphy: Example from the Castlegate Sandstone, central Utah, U.S.A. *Journal of Sedimentary Research*, *82*(2), 121-130. DOI:10.2110/jsr.2012.8

Hansford, M. R., Plink-Björklund, P., & Jones, E. R. (2020). Global quantitative analyses of river discharge variability and hydrograph shape with respect to climate types. *Earth-Science Reviews*, *200*, 102977. DOI:10.1016/j.earscirev.2019.102977

Hay, W., L. Eicher, D., & Diner, R. (1993). Physical oceanography and water masses of the Cretaceous Western Interior Seaway. In W. E. G. Caldwell & E. G. Kauffman (Eds.), *Evolution of the Western Interior Basin* (pp. 297-318). Geological Association of Canada.

Hayden, A. T., Lamb, M. P., & McElroy, B. J. (2021a). Constraining the timespan of fluvial activity from the intermittency of sediment transport on Earth and Mars. *Geophysical Research Letters*, *n/a*(n/a), e2021GL092598. DOI:10.1029/2021GL092598

Hayden, A. T., Lamb, M. P., Myrow, P. M., Mohrig, D., Williams, R. M. E., Cuevas Martínez, J. L., Cardenas, B. T., Findlay, C. P., Ewing, R. C., & McElroy, B. J. (2021b). The Oligocene-Miocene Guadalope-Matarranya Fan, Spain, as an Analog for Long-Lived, Ridge-Bearing Megafans on Mars. *Journal of Geophysical Research: Planets*, *126*(12), e2021JE006993. DOI:10.1029/2021JE006993

Herbert, C. M., Alexander, J., Amos, K. J., & Fielding, C. R. (2020). Unit bar architecture in a highly-variable fluvial discharge regime: Examples from the Burdekin River, Australia. *Sedimentology*, *67*(1), 576-605. DOI:10.1111/sed.12655

Hilton, R. G., Galy, A., Hovius, N., Chen, M.-C., Horng, M.-J., & Chen, H. (2008). Tropical-cyclone-driven erosion of the terrestrial biosphere from mountains. *Nature Geoscience*, *1*(11), 759-762. DOI:10.1038/ngeo333

Holbrook, J., & Wanas, H. (2014). A fulcrum approach to assessing source-to-sink mass balance using channel paleohydrologic paramaters derivable from common fluvial data sets with an example from the Cretaceous of Egypt. *Journal of Sedimentary Research*, *84*(5), 349-372. DOI:10.2110/jsr.2014.29

Holbrook, J. M., & Miall, A. D. (2020). Time in the Rock: A field guide to interpreting past events and processes from siliciclastic stratigraphy. *Earth-Science Reviews*, *203*, 103121. DOI:10.1016/j.earscirev.2020.103121

Hovius, N. (1996). Regular spacing of drainage outlets from linear mountain belts. *Basin Research*, *8*(1), 29-44. DOI:10.1111/j.1365-2117.1996.tb00113.x

Jarrard, R. D., Sondergeld, C. H., Chan, M. A., & Erickson, S. N. (2004). Petrophysics of the Cretaceous Ferron Sandstone, Central Utah. In T. C. Chidsey, Jr., R. D. Adams, & T. H. Morris (Eds.), *Regional to Wellbore Analog for Fluvial-Deltaic Reservoir Modeling: The Ferron Sandstone of Utah* (Vol. 50, pp. 0). American Association of Petroleum Geologists. https://doi.org/10.1306/St50983

Jerolmack, D. J., Mohrig, D., Zuber, M. T., & Byrne, S. (2004). A minimum time for the formation of Holden Northeast fan, Mars. *Geophysical Research Letters*, *31*(21). DOI:10.1029/2004GL021326

Juez, C., Garijo, N., Hassan, M. A., & Nadal-Romero, E. (2021). Intraseasonal-to-Interannual Analysis of Discharge and Suspended Sediment Concentration Time-Series of the Upper Changjiang (Yangtze River). *Water Resources Research*, *57*(8), e2020WR029457. DOI:10.1029/2020WR029457

Kamada, A., Kuroda, T., Kasaba, Y., Terada, N., Nakagawa, H., & Toriumi, K. (2020). A coupled atmosphere–hydrosphere global climate model of early Mars: A 'cool and wet' scenario for the formation of water channels. *Icarus*, *338*, 113567. DOI:10.1016/j.icarus.2019.113567

Kauffman, E. G. (1977). Geological and biological overview: Western Interior Basin In E. G. Kauffman (Ed.), *Cretaceous facies, faunas, and paleoenvironments across the Western Interior Basin* (pp. 75-99). Rocky Mountain Association of Geologists.

Kauffman, E. G., & Caldwell, W. (1993). The Western Interior Basin in space and time. In E. G. Kauffman & W. Caldwell (Eds.), *Evolution of the Western Interior Basin: Geological Association of Canada, Special Paper 39* (pp. 1-30).

Kitoh, A., Motoi, T., & Arakawa, O. (2010). Climate modelling study on mountain uplift and Asian monsoon evolution. *Geological Society, London, Special Publications*, *342*(1), 293. DOI:10.1144/SP342.17

Kleinhans, M. G. (2005). Flow discharge and sediment transport models for estimating a minimum timescale of hydrological activity and channel and delta formation on Mars. *Journal of Geophysical Research: Planets*, *110*(E12). DOI:10.1029/2005JE002521

Kynaston, D. (2019). *Stratigraphy, provenance, timing and control of incised valleys in the Ferron Sandstone* McMaster University]. http://hdl.handle.net/11375/25035

Lapôtre, M. G. A., & Ielpi, A. (2020). The pace of fluvial meanders on Mars and implications for the western delta deposits of Jezero Crater. *AGU Advances*, *1*(2), e2019AV000141. DOI:10.1029/2019AV000141

Leithold, E. L., Blair, N. E., & Wegmann, K. W. (2016). Source-to-sink sedimentary systems and global carbon burial: A river runs through it. *Earth-Science Reviews*, *153*, 30-42. DOI:10.1016/j.earscirev.2015.10.011

Lemma, H., Nyssen, J., Frankl, A., Poesen, J., Adgo, E., & Billi, P. (2019). Bedload transport measurements in the Gilgel Abay River, Lake Tana Basin, Ethiopia. *Journal of Hydrology*, *577*, 123968. DOI:10.1016/j.jhydrol.2019.123968

Li, Y., Bhattacharya, J. P., Ahmed, S., & Garza, D. (2018). Re-evaluating the paleogeography of the river-dominated and wave-influenced Ferron Notom Delta, Southern Central Utah: an integration of detailed facies-architecture and paleocurrent analysis. *Journal of Sedimentary Research*, *88*(2), 214-240. DOI:10.2110/jsr.2018.9

Lin, W., & Bhattacharya, J. P. (2017). Estimation of source-to-sink mass balance by a fulcrum approach using channel paleohydrologic parameters of the Cretaceous Dunvegan Formation, Canada. *Journal of Sedimentary Research*, *87*(1), 97-116. DOI:10.2110/jsr.2017.1

Liu, Y., Xinyu, L., Liancheng, Z., Yang, L., Chunrong, J., Ni, W., & Juan, Z. (2021). Quantifying rain, snow and glacier meltwater in river discharge during flood events in the Manas River Basin, China. *Natural Hazards*, *108*(1), 1137-1158. DOI:10.1007/s11069-021-04723-8

Lunt, D., Farnsworth, A., Loptson, C., Foster, G., Markwick, P., O'Brien, C., Pancost, R. D., Robinson, S. A., & Wrobel, N. (2016). Palaeogeographic controls on climate and proxy interpretation. *Climate of the Past*, *12*, 1181-1198. DOI:10.5194/cpd-11-5683-2015

Lyster, S. J., Whittaker, A. C., Allison, P. A., Lunt, D. J., & Farnsworth, A. (2020). Predicting sediment discharges and erosion rates in deep time—examples from the late Cretaceous North American continent. *Basin Research*, *32*(6), 1547-1573. DOI:10.1111/bre.12442

Lyster, S. J., Whittaker, A. C., & Hajek, E. A. (2022a). The problem of paleo-planforms. *Geology*, *50*, 822-826. DOI:10.1130/G49867.1

Lyster, S. J., Whittaker, A. C., Hajek, E. A., & Ganti, V. (2022b). Field evidence of bedform disequilibrium dynamics in preserved fluvial cross-strata: Discharge variability or morphodynamic hierarchy? *Earth and Planetary Science Letters*, *579*, 117355. DOI:10.1016/j.epsl.2021.117355

Lyster, S. J., Whittaker, A. C., Hampson, G. J., Hajek, E. A., Allison, P. A., & Lathrop, B. A. (2021). Reconstructing the morphologies and hydrodynamics of ancient rivers from source to sink: Cretaceous Western Interior Basin, Utah, USA. *Sedimentology*, *68*(6), 2854-2886. DOI:10.1111/sed.12877

Mack, G. H., & James, W. C. (1994). Paleoclimate and the global distribution of paleosols. *The Journal of Geology*, *102*(3), 360-366. DOI:10.1086/629677

Mack, G. H., James, W. C., & Monger, H. C. (1993). Classification of paleosols. *GSA Bulletin*, *105*(2), 129-136. DOI:10.1130/0016-7606(1993)105<0129:COP>2.3.CO;2

Mahon, R. C., & McElroy, B. (2018). Indirect estimation of bedload flux from modern sand-bed rivers and ancient fluvial strata. *Geology*, *46*(7), 579-582. DOI:10.1130/G40161.1

Markwick, P. J. (2018). Palaeogeography in exploration. *Geological Magazine*, *156*, 366-407. DOI:10.1017/S0016756818000468

Markwick, P. J., & Valdes, P. J. (2004). Palaeo-digital elevation models for use as boundary conditions in coupled ocean–atmosphere GCM experiments: a Maastrichtian (late Cretaceous) example. *Palaeogeography, Palaeoclimatology, Palaeoecology*, *213*(1-2), 37-63. DOI:10.1016/j.palaeo.2004.06.015

Marzocchi, A., Lunt, D. J., Flecker, R., Bradshaw, C. D., Farnsworth, A., & Hilgen, F. J. (2015). Orbital control on late Miocene climate and the North African monsoon: insight from an ensemble of sub-precessional simulations. *Clim. Past*, *11*(10), 1271-1295. DOI:10.5194/cp-11-1271-2015

McCabe, P. J., & Parrish, J. T. (1992). Tectonic and climatic controls on the distribution and quality of Cretaceous coals. In P. J. McCabe & J. T. Parrish (Eds.), *Controls on the Distribution and Quality of Cretaceous Coals* (Vol. 267, pp. 0). Geological Society of America. https://doi.org/10.1130/SPE267-p1

Metz, J. M., Grotzinger, J. P., Mohrig, D., Milliken, R., Prather, B., Pirmez, C., McEwen, A. S., & Weitz, C. M. (2009). Sublacustrine depositional fans in southwest Melas Chasma. *Journal of Geophysical Research: Planets*, *114*(E10). DOI:10.1029/2009JE003365

Meybeck, M., Laroche, L., Dürr, H. H., & Syvitski, J. P. M. (2003). Global variability of daily total suspended solids and their fluxes in rivers. *Global and Planetary Change*, *39*(1), 65-93. DOI:10.1016/S0921-8181(03)00018-3

Molenaar, C. M., & Cobban, W. A. (1991). Middle Cretaceous stratigraphy on the south side of the Uinta Basin, east-central Utah. In T. C. Chidsey Jr (Ed.), *Geology of east-central Utah* (Vol. 19, pp. 29-43). Utah Geological Association.

Moore, J. M., Howard, A. D., Dietrich, W. E., & Schenk, P. M. (2003). Martian Layered Fluvial Deposits: Implications for Noachian Climate Scenarios. *Geophysical Research Letters*, *30*(24). DOI:10.1029/2003GL019002

Moramarco, T., Saltalippi, C., & Singh, V. P. (2011). Velocity profiles assessment in natural channels during high floods. *Hydrology Research*, *42*(2-3), 162-170. DOI:10.2166/nh.2011.064

Najibi, N., & Devineni, N. (2017). Recent trends in frequency and duration of global floods. *Earth System Dynamics Discussions*, *9*, 757-783. DOI:10.5194/esd-2017-59

Namsai, M., Bidorn, B., Chanyotha, S., Mama, R., & Phanomphongphaisarn, N. (2020). Sediment dynamics and temporal variation of runoff in the Yom River, Thailand. *International Journal of Sediment Research*, *35*. DOI:10.1016/j.ijsrc.2020.03.002

Neal, E. G., Todd Walter, M., & Coffeen, C. (2002). Linking the pacific decadal oscillation to seasonal stream discharge patterns in Southeast Alaska. *Journal of Hydrology*, *263*(1), 188-197. DOI:10.1016/S0022-1694(02)00058-6

Obradovich, J. D. (1993). A Cretaceous time scale. In W. E. G. Caldwell & E. Kauffman (Eds.), *Evolution of the Western Interior Basin* (Vol. Special Paper 39, pp. 379-396). Geological Association of Canada.

Paola, C., Ganti, V., Mohrig, D., Runkel, A. C., & Straub, K. M. (2018). Time not our time: Physical controls on the preservation and measurement of geologic time. *Annual Review of Earth and Planetary Sciences*, *46*(1), 409-438. DOI:10.1146/annurev-earth-082517-010129

Paola, C., Heller, P., & Angevine, C. (1992). The large-scale dynamics of grain-size variation in alluvial basins, 1: Theory. *Basin Research*, *4*(2), 73-90. DOI:10.1111/j.1365-2117.1992.tb00145.x

Parrish, J., & Barron, E. J. (1986). Paleoclimates and economic geology. *SEPM Short Course*, *18*, 1-162.

Parrish, J. T., Ziegler, A. M., & Scotese, C. R. (1982). Rainfall patterns and the distribution of coals and evaporites in the Mesozoic and Cenozoic. *Palaeogeography, Palaeoclimatology, Palaeoecology*, *40*(1), 67-101. DOI:10.1016/0031-0182(82)90085-2

Pasquini, A. I., & Depetris, P. J. (2007). Discharge trends and flow dynamics of South American rivers draining the southern Atlantic seaboard: An overview. *Journal of Hydrology*, *333*(2), 385-399. DOI:10.1016/j.jhydrol.2006.09.005

Plink-Björklund, P. (2015). Morphodynamics of rivers strongly affected by monsoon precipitation: Review of depositional style and forcing factors. *Sedimentary Geology*, *323*, 110-147. DOI:10.1016/j.sedgeo.2015.04.004

Pujalte, V., Schmitz, B., & Payros, A. (2022). A rapid sedimentary response to the Paleocene-Eocene Thermal Maximum hydrological change: New data from alluvial units of the Tremp-Graus Basin (Spanish Pyrenees). *Palaeogeography, Palaeoclimatology, Palaeoecology*, *589*, 110818. DOI:10.1016/j.palaeo.2021.110818

Ramirez, R. M., Craddock, R. A., & Usui, T. (2020). Climate Simulations of Early Mars With Estimated Precipitation, Runoff, and Erosion Rates. *Journal of Geophysical Research: Planets*, *125*(3), e2019JE006160. DOI:10.1029/2019JE006160

Rîmbu, N., Boroneanţ, C., Buţă, C., & Dima, M. (2002). Decadal variability of the Danube river flow in the lower basin and its relation with the North Atlantic Oscillation. *International Journal of Climatology*, *22*(10), 1169-1179. DOI:10.1002/joc.788

Roberts, L. N. R., & Kirschbaum, M. A. (1995). Paleogeography and the Late Cretaceous of the Western Interior of middle North America: coal distribution and sediment accumulation [Report]. *U.S. Geological Survey Professional Paper*, *1561*, 1-65. DOI:10.3133/pp1561

Romans, B. W., Castelltort, S., Covault, J. A., Fildani, A., & Walsh, J. P. (2016). Environmental signal propagation in sedimentary systems across timescales. *Earth-Science Reviews*, *153*, 7-29. DOI:10.1016/j.earscirev.2015.07.012

Rood, S. B., Foster, S. G., Hillman, E. J., Luek, A., & Zanewich, K. P. (2016). Flood moderation: Declining peak flows along some Rocky Mountain rivers and the underlying mechanism. *Journal of Hydrology*, *536*, 174-182. DOI:10.1016/j.jhydrol.2016.02.043

Ryer, T. A., & Anderson, P. B. (2004). Facies of the Ferron Sandstone, East-Central Utah. In T. C. Chidsey, Jr., R. D. Adams, & T. H. Morris (Eds.), *Regional to Wellbore Analog for Fluvial-Deltaic Reservoir Modeling: The Ferron Sandstone of Utah* (Vol. 50, pp. 0). American Association of Petroleum Geologists. https://doi.org/10.1306/St50983

Sadeghi, S. H., & Kheirfam, H. (2015). Temporal Variation of Bed Load to Suspended Load Ratio in Kojour River, Iran. *CLEAN – Soil, Air, Water*, *43*(10), 1366-1374. DOI:10.1002/clen.201400490

Sadler, P. M. (1981). Sediment accumulation rates and the completeness of stratigraphic sections. *The Journal of Geology*, *89*, 569-584. DOI:10.1086/628623

Sadler, P. M. (1993). Time scale dependence of the rates of unsteady geologic processes. In J. M. Armentrout, R. Bloch, H. C. Olson, & B. F. Perkins (Eds.), *Rates of Geologic Processes, Tectonics, Sedimentation, Eustasy and Climate–Implications for Hydrocarbon Exploration*. SEPM Society for Sedimentary Geology. https://doi.org/10.5724/gcs.93.14.0221

Serinaldi, F., Loecker, F., Kilsby, C. G., & Bast, H. (2018). Flood propagation and duration in large river basins: a data-driven analysis for reinsurance purposes. *Natural Hazards*, *94*(1), 71-92. DOI:10.1007/s11069-018-3374-0

Sewall, J. O., & Fricke, H. C. (2013). Andean-scale highlands in the Late Cretaceous Cordillera of the North American western margin. *Earth and Planetary Science Letters*, *362*, 88-98. DOI:10.1016/j.epsl.2012.12.002

Shanley, K. W., & McCabe, P. J. (1995). Sequence Stratigraphy of Turonian–Santonian Strata, Kaiparowits Plateau, Southern Utah, U.S.A.: Implications for Regional Correlation and Foreland Basin Evolution. In J. C. V. Wagoner & G. T. Bertram (Eds.), *Sequence Stratigraphy of Foreland Basin Deposits: Outcrop and Subsurface Examples from the Cretaceous of North America* (Vol. 64, pp. 0). American Association of Petroleum Geologists. https://doi.org/10.1306/M64594C6

Sharma, S., Bhattacharya, J. P., & Richards, B. (2017). Source-to-sink sediment budget analysis of the Cretaceous Ferron Sandstone, Utah, U.S.A., using the fulcrum approach. *Journal of Sedimentary Research*, *87*(6), 594-608. DOI:10.2110/jsr.2017.23

Simpson, H. J., Cane, M. A., Herczeg, A. L., Zebiak, S. E., & Simpson, J. H. (1993). Annual river discharge in southeastern Australia related to El Nino-Southern Oscillation forecasts of sea surface temperatures. *Water Resources Research*, *29*(11), 3671-3680. DOI:10.1029/93WR01492

Sklar, L. S., & Dietrich, W. E. (2004). A mechanistic model for river incision into bedrock by saltating bed load. *Water Resources Research*, *40*(6). DOI:10.1029/2003WR002496

Snell, K. E., Koch, P. L., Druschke, P., Foreman, B. Z., & Eiler, J. M. (2014). High elevation of the 'Nevadaplano' during the Late Cretaceous. *Earth and Planetary Science Letters*, *386*, 52-63. DOI:10.1016/j.epsl.2013.10.046

Steakley, K., Murphy, J., Kahre, M., Haberle, R., & Kling, A. (2019). Testing the impact heating hypothesis for early Mars with a 3-D global climate model. *Icarus*, *330*, 169-188. DOI:10.1016/j.icarus.2019.04.005

Stephenson, S. N., Roberts, G. G., Hoggard, M. J., & Whittaker, A. C. (2014). A Cenozoic uplift history of Mexico and its surroundings from longitudinal river profiles. *Geochemistry, Geophysics, Geosystems*, *15*(12), 4734-4758. DOI:10.1002/2014GC005425

Stucky de Quay, G., Kite, E. S., & Mayer, D. P. (2019). Prolonged fluvial activity from channel-fan systems on Mars. *Journal of Geophysical Research: Planets*, *124*(11), 3119-3139. DOI:10.1029/2019JE006167

Sun, H., & Furbish, D. J. (1997). Annual precipitation and river discharges in Florida in response to El Niño- and La Niña-sea surface temperature anomalies. *Journal of Hydrology*, *199*(1), 74-87. DOI:10.1016/S0022-1694(96)03303-3

Syvitski, J. P. M., & Milliman, J. D. (2007). Geology, geography, and humans battle for dominance over the delivery of fluvial sediment to the coastal ocean. *The Journal of Geology*, *115*(1), 1-19. DOI:10.1086/509246

Tabor, C. R., Poulsen, C. J., Lunt, D. J., Rosenbloom, N. A., Otto-Bliesner, B. L., Markwick, P. J., Brady, E. C., Farnsworth, A., & Feng, R. (2016). The cause of Late Cretaceous cooling: A multimodel-proxy comparison. *Geology*, *44*(11), 963-966. DOI:10.1130/g38363.1

Tabor, N., & Myers, T. (2014). Paleosols as Indicators of Paleoenvironment and Paleoclimate. *Annual Review of Earth and Planetary Sciences*, *43*, 150317182938004. DOI:10.1146/annurev-earth-060614-105355

Tabor, N. J., Montañez, I. P., Scotese, C. R., Poulsen, C. J., & Mack, G. H. (2008). Paleosol archives of environmental and climatic history in paleotropical western Pangea during the latest Pennsylvanian through

Early Permian. In C. R. Fielding, T. D. Frank, & J. L. Isbell (Eds.), *Resolving the Late Paleozoic Ice Age in Time and Space* (Vol. 441, pp. 0). Geological Society of America. https://doi.org/10.1130/2008.2441(20)

Tachibana, Y., Oshima, K., & Ogi, M. (2008). Seasonal and interannual variations of Amur River discharge and their relationships to large-scale atmospheric patterns and moisture fluxes. *Journal of Geophysical Research: Atmospheres*, *113*(D16). DOI:10.1029/2007JD009555

Tindall, J., Flecker, R., Valdes, P., Schmidt, D. N., Markwick, P., & Harris, J. (2010). Modelling the oxygen isotope distribution of ancient seawater using a coupled ocean–atmosphere GCM: Implications for reconstructing early Eocene climate. *Earth and Planetary Science Letters*, *292*(3-4), 265-273. DOI:10.1016/j.epsl.2009.12.049

Trampush, S. M., Huzurbazar, S., & McElroy, B. (2014). Empirical assessment of theory for bankfull characteristics of alluvial channels. *Water Resources Research*, *50*(12), 9211-9220. DOI:10.1002/2014WR015597

Valdes, P. J., Armstrong, E., Badger, M. P. S., Bradshaw, C. D., Bragg, F., Crucifix, M., Davies-Barnard, T., Day, J. J., Farnsworth, A., Gordon, C., Hopcroft, P. O., Kennedy, A. T., Lord, N. S., Lunt, D. J., Marzocchi, A., Parry, L. M., Pope, V., Roberts, W. H. G., Stone, E. J., Tourte, G. J. L., & Williams, J. H. T. (2017). The BRIDGE HadCM3 family of climate models: HadCM3@Bristol v1.0. *Geoscientific Model Development*, *10*(10), 3715-3743. DOI:10.5194/gmd-10-3715-2017

van den Bergh, T. C. V., & Garrison, J. R. (2004). *Effects of changes in rate of sedimentation and relative change in sea-level on the geometry, architecture, and sedimentology of fluvial and deltaic sandstones within the Upper Ferron Sandstone Last Chance Delta, East-Central Utah: implications for reservoir modeling* (Vol. 50).

van Rijn, L. C. (1984). Sediment transport, part II: Suspended load transport. *Journal of Hydraulic Engineering*, *110*(11), 1613-1641. DOI:10.1061/(ASCE)0733-9429(1984)110:11(1613)

Wang, J., & Plink-Björklund, P. (2020). Variable-discharge-river macroforms in the Sunnyside Delta Interval of the Eocene Green River Formation, Uinta Basin, USA. *Sedimentology*, *67*(4), 1914-1950. DOI:10.1111/sed.12688

Watkins, S. E. (2019). *Linking source and sink in an active rift: quantifying controls on sediment export and depositional stratigraphy in the Gulf of Corinth, central Greece* Imperial College London].

Watkins, S. E., Whittaker, A., Ganti, V., Bell, R., Brooke, S., Gawthorpe, R., & McNeill, L. (2018a). Quantifying sediment dynamics and intermittency of gravel bed rivers; examples from the Gulf of Corinth. *EGU General Assembly Conference Abstracts*, 19573. https://ui.adsabs.harvard.edu/abs/2018EGUGA..2019573W

Watkins, S. E., Whittaker, A. C., Bell, R. E., McNeill, L. C., Gawthorpe, R. L., Brooke, S. A. S., & Nixon, C. W. (2018b). Are landscapes buffered to high-frequency climate change? A comparison of sediment fluxes and depositional volumes in the Corinth Rift, central Greece, over the past 130 k.y. *GSA Bulletin*, *131*, 372-388. DOI:10.1130/B31953.1

Wentworth, C. K. (1922). A scale of grade and class terms for clastic sediments. *The Journal of Geology*, *30*(5), 377-392. DOI:10.1086/622910

Williams, G. P. (1978). Bank-full discharge of rivers. *Water Resources Research*, *14*(6), 1141-1154. DOI:10.1029/WR014i006p01141

Wolman, M. G. (1954). A method of sampling coarse river-bed material. *Eos Transactions American Geophysical Union*, *35*(6), 951-956. DOI:10.1029/TR035i006p00951

Wolman, M. G., & Miller, J. P. (1960). Magnitude and Frequency of Forces in Geomorphic Processes. *The Journal of Geology*, *68*(1), 54-74. DOI:10.1086/626637

Wood, J., McLeod Jonah, S., Lyster Sinéad, J., & Whittaker Alexander, C. (2022). Rivers of the Variscan Foreland: fluvial morphodynamics in the Pennant Formation of South Wales, UK. *Journal of the Geological Society*, *0*(ja), jgs2022-2048. DOI:10.1144/jgs2022-048

Woodyer, K. D. (1968). Bankfull frequency in rivers. *Journal of Hydrology*, *6*(2), 114-142. DOI:10.1016/0022-1694(68)90155-8

Wordsworth, R. D. (2016). The Climate of Early Mars. *Annual Review of Earth and Planetary Sciences*, *44*(1), 381-408. DOI:10.1146/annurev-earth-060115-012355

Wordsworth, R. D., Kerber, L., Pierrehumbert, R. T., Forget, F., & Head, J. W. (2015). Comparison of "warm and wet" and "cold and icy" scenarios for early Mars in a 3-D climate model. *Journal of Geophysical Research: Planets*, *120*(6), 1201-1219. DOI:10.1002/2015JE004787

Wright, S., & Parker, G. (2004). Flow resistance and suspended load in sand-bed rivers: Simplified stratification model. *Journal of Hydraulic Engineering*, *130*(8), 796-805. DOI:10.1061/(ASCE)0733-9429(2004)130:8(796)

Wright, S., & Parker, G. (2005). Modeling downstream fining in sand-bed rivers. I: formulation. *Journal of Hydraulic Research*, *43*(6), 613-620. DOI:10.1080/00221680509500381

Wu, C., Bhattacharya, J. P., & Ullah, M. S. (2015). Paleohydrology and 3D Facies Architecture of Ancient Point Bars, Ferron Sandstone, Notom Delta, South-Central Utah, U.S.A. *Journal of Sedimentary Research*, *85*(4), 399-418. DOI:10.2110/jsr.2015.29

Zhang, J., Covault, J., Pyrcz, M., Sharman, G., Carvajal, C., & Milliken, K. (2018). Quantifying sediment supply to continental margins: Application to the Paleogene Wilcox Group, Gulf of Mexico. *AAPG Bulletin*, *102*(9), 1685-1702. DOI:10.1306/01081817308

Zhang, W., Mu, S.-s., Zhang, Y.-j., & Chen, K.-m. (2012). Seasonal and interannual variations of flow discharge from Pearl River into sea. *Water Science and Engineering*, *5*(4), 399-409. DOI:10.3882/j.issn.1674-2370.2012.04.004
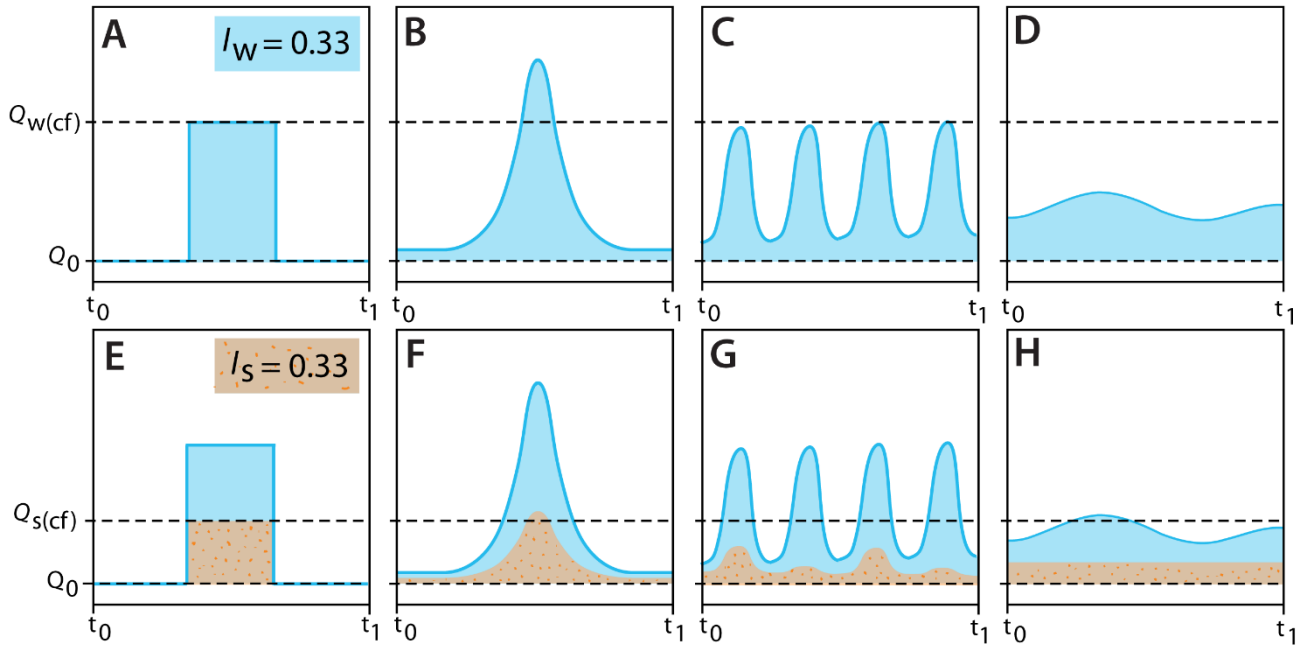
Figure 1: Schematic illustrating the flow intermittency factor, I_w, and sediment transport intermittency factor, I_s (not to scale). On y-axes, Q is discharge, with Q_0 = zero discharge (of both water and sediment), $Q_{w(cf)}$ = channel-forming water discharge, and $Q_{s(cf)}$ = channel-forming sediment flux. On x-axes, t is time, with t_0 = start time and t_1 = end time. t_0–t_1 can be any time length, e.g., one year, ten years, etc. The x-axes therefore reflect theoretical hydrographs which, depending on t_0–t_1, could be annual or decadal hydrographs, etc. **A)** An I_w value of 0.33 implies that a river could transport the same amount of water it transports during the real hydrograph in 0.33 of the time if channel-forming conditions are sustained. This assumes that Q_w=0 for the remaining length of the hydrograph. Given that Q_w=0 is unlikely, parts **B–D** illustrate potential river hydrographs that could also reflect I_w=0.33. These potential river hydrographs assume some form of base flow. **E)** An I_s value of 0.33 implies that a river could transport the same amount of sediment it transports during the real hydrograph in 0.33 of the time, if channel-forming conditions are sustained, and assuming that channel-forming conditions do geomorphic work. This assumes that Q_s=0 for the remaining length of the hydrograph. Similarly, Q_s=0 is unlikely, and parts **F–H** illustrate potential distributions of sediment transport across the hydrograph that could also reflect I_s=0.33.
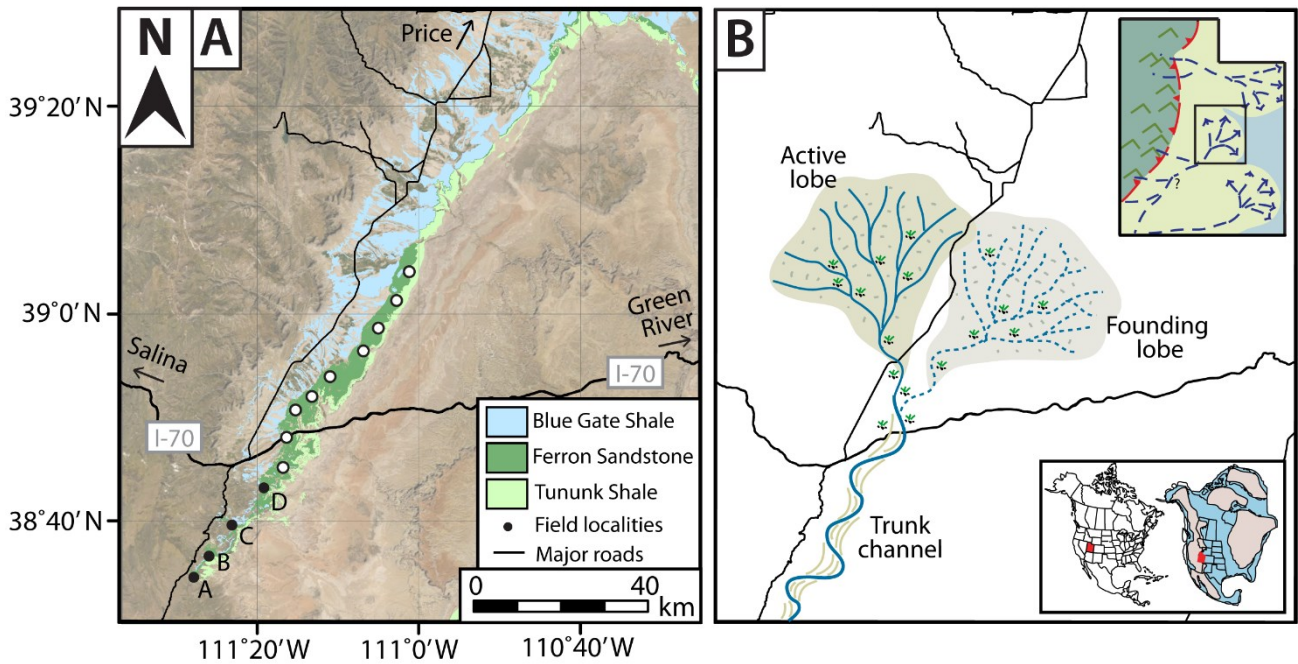
Figure 2: A) Map of study area in central Utah, USA, including outcrop of the Last Chance Ferron Sandstone (forest green), stratigraphically older Tununk Shale (light green), and stratigraphically younger Blue Gate Shale (light blue). Black-outlined, black-filled circles (labelled A–D) indicate the field localities visited in this study, and black-outlined, white-filled circles (no labels) are points of geographic reference in Figure 3 and were not visited in this study. **B)** Paleogeographic reconstruction of the study area, adapted from Cotter (1976). Major roads are depicted to facilitate geographic orientation. Top right inset shows a schematic paleogeography of Utah during the Turonian (Late Cretaceous); the black box indicates the approximate position and extent of parts A/B. Bottom right inset shows the location of Utah relative to the modern North American continent (left) and Late Cretaceous North American continent (right).
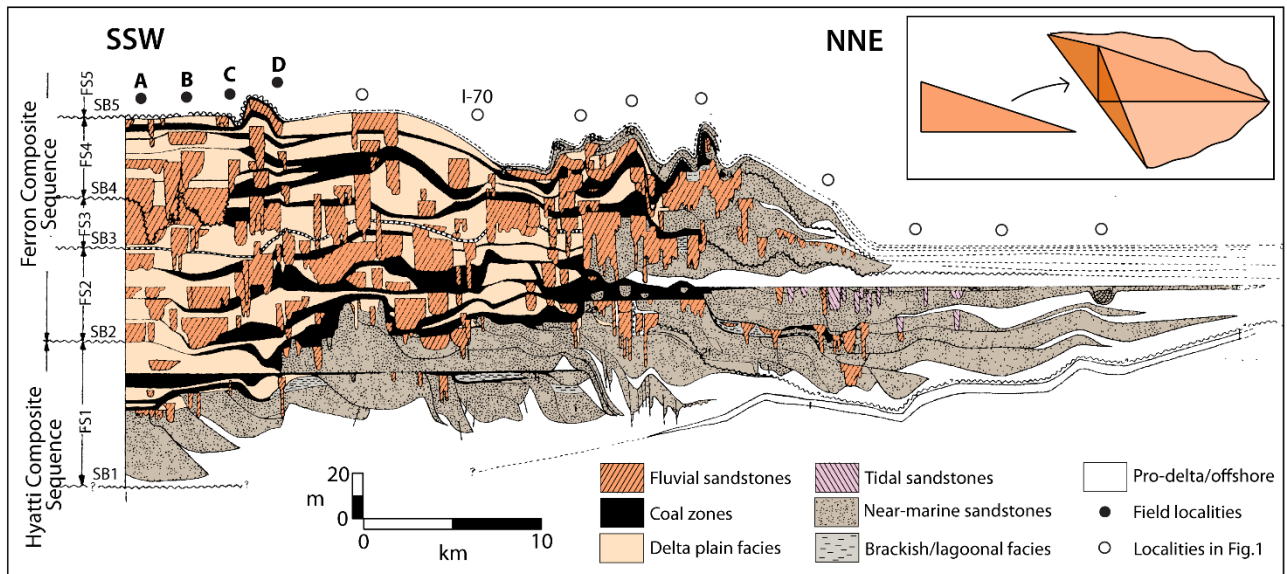
Figure 3: Depositional sequence stratigraphy of the Last Chance Ferron Sandstone (adapted from Garrison Jr and van den Bergh (2004). Black-outlined, black-filled circles (labelled A–D) indicate the locations of field localities in this study (see Figure 2), and black-outlined, white-filled circles (no labels) are points of geographic reference indicated in Figure 2. Inset shows how we used the depositional sequence stratigraphy to estimate the total depositional volume of the Last Chance Ferron Sandstone. Refer to Garrison Jr and van den Bergh (2004) for details pertaining to FS1–FS5 and SB1–SB5 notations, as well as information pertaining to the Ferron and Hyatti composite sequences and the illustrated sequence boundaries.
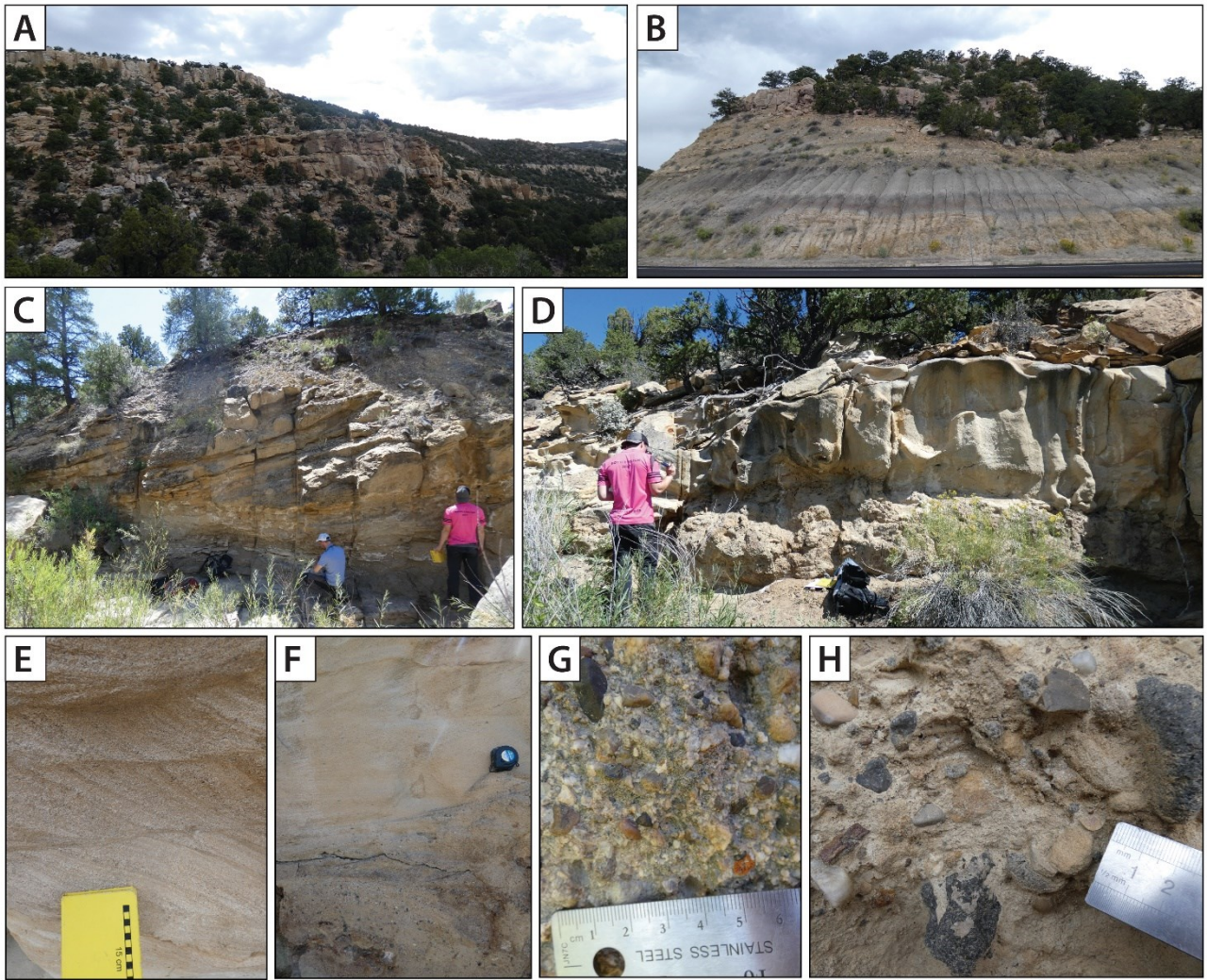
Figure 4: Typical exposure of the Last Chance Ferron Sandstone at paleo-landward field localities. **A)** Major channelized fluvial sandstone bodies are surrounded by abundant floodplain fines (typically vegetated). Maximum height of the multistory channelized fluvial sandstone body in the center of the photo is ~10 m. **B)** Low chroma hydromorphic paleosols, interspersed with thin sandstones, situated beneath a major channelized fluvial sandstone body. Vertical height of cliff face is ~45 m. **C)** Barform scale accretion in a channelized fluvial sandstone body. **D)** Channelized fluvial sandstone body in which the upper section is characterized by cross-bedded sand-grade sediments, and the lower section is characterized by moderate to poorly sorted gravel-grade sediments. **E)** Dune-scale cross-stratification in sand to granule-grade deposits. **F)** Dune-scale cross-stratification in sand-grade deposits (upper section) and granule- to gravel-grade deposits (lower section). **G)** Moderate to poorly sorted conglomerates. **H)** Poorly sorted conglomerates.
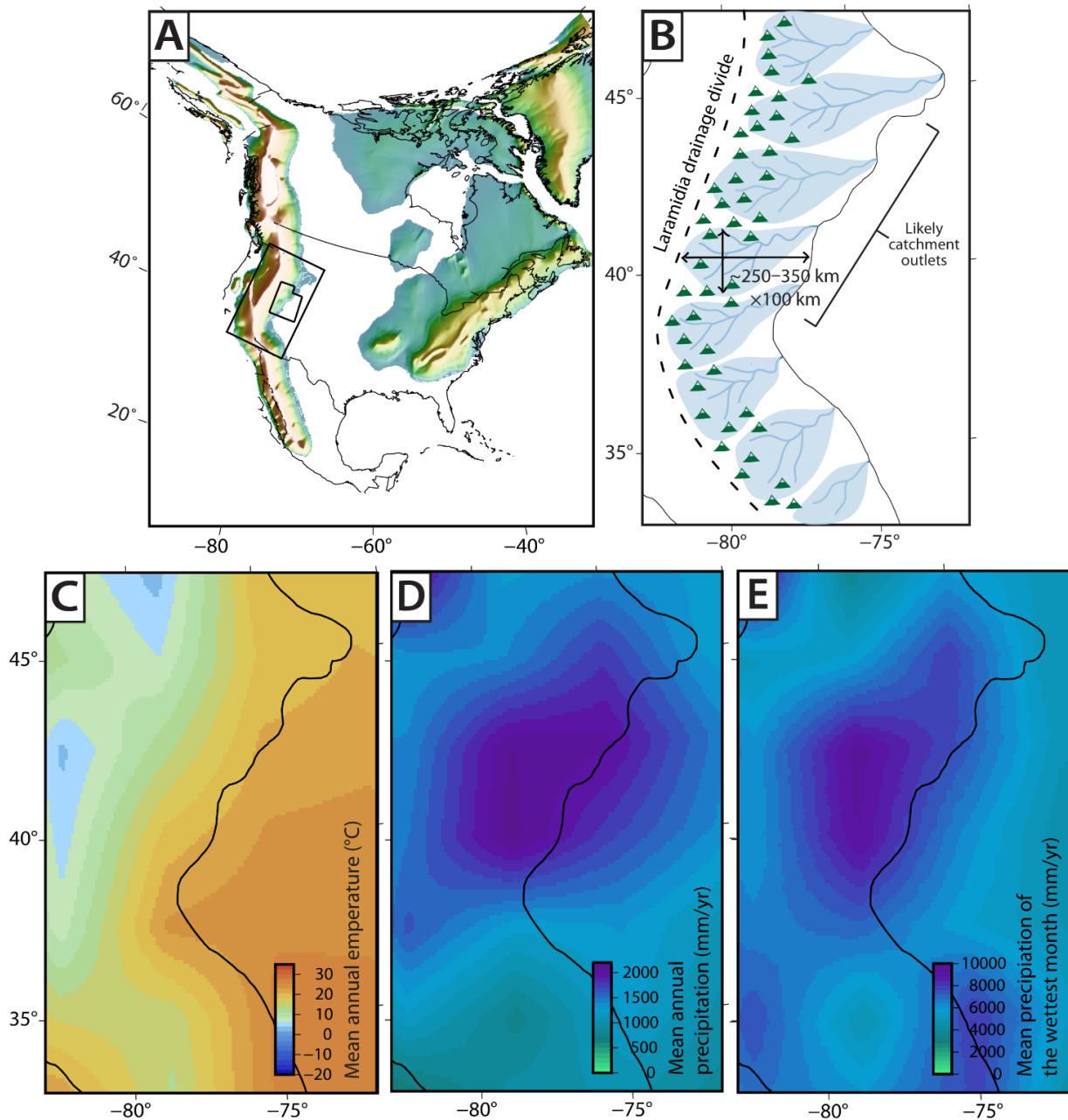
Figure 5: Paleogeographic and paleoclimatic constraints implemented in this study. **A)** Paleo-topographic reconstruction of the Turonian (Late Cretaceous) North American continent. Adapted from Figure 1 in Lyster et al. (2020). Solid black lines reflect modern North American coastlines and country borders. The black box indicates the approximate position and extent of parts B–E, inside which is a black polygon indicating the approximate position and extent of Utah state. **B)** Schematic paleogeography of the study area indicating the approximate sizes and configurations of paleo-catchments in the Western Interior during the Turonian stage of the Late Cretaceous. Paleo-catchment configurations are approximated following Gardner (1995); Bhattacharya and Tye (2004); Ryer and Anderson (2004); Bhattacharya et al. (2016); Kynaston (2019); Lyster et al. (2020). The solid black line indicates the position of the highstand paleoshoreline (extracted from part A; c.f. Lyster et al. (2020)), and the dashed black line indicates the approximate position of the regional drainage divide. **C)** HadCM3L general circulation model (GCM) predictions of mean annual air temperature (at 1.5 m above the local surface). **D)** HadCM3L GCM predictions of mean annual precipitation. **E)** HadCM3L GCM predictions of mean precipitation of the wettest month of a simulated year.
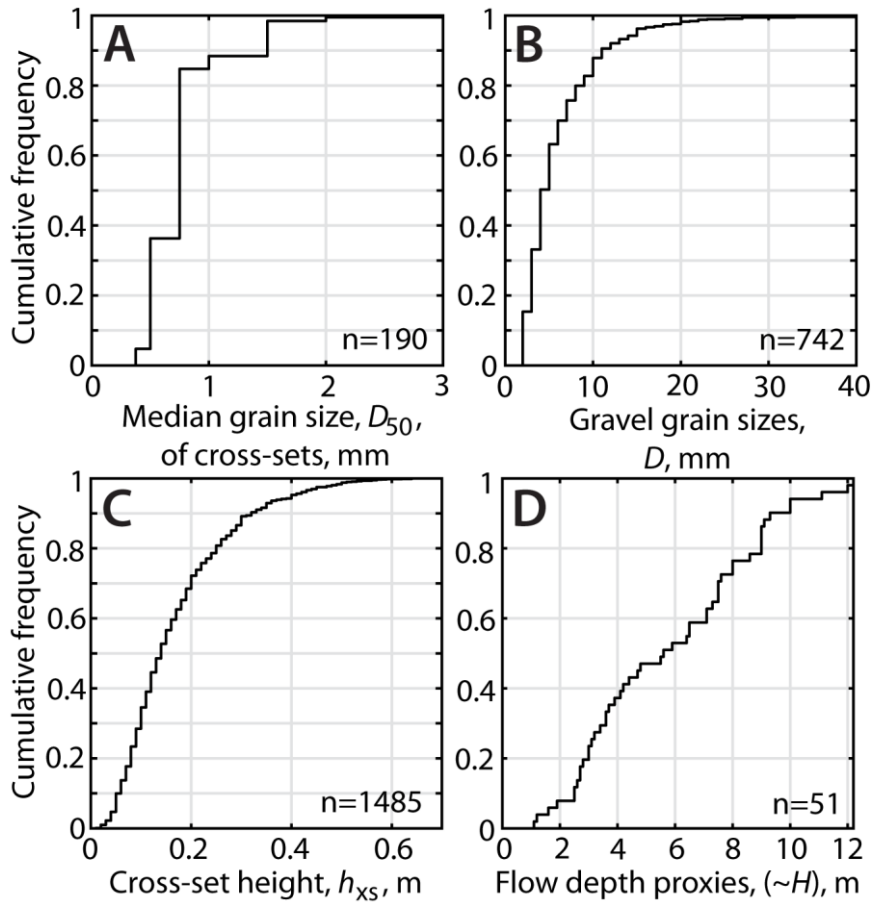
Figure 6: Summary of field measurements collected from terrestrial fluvial strata of the Last Chance Ferron Sandstone. **A)** The cumulative frequency of median grain-size estimates for n=190 individual cross-sets. **B)** The cumulative frequency of gravel grain size measurements obtained from gravel horizons and lenses (n=742 from 8 counts of ≤100 measurements). **C)** The cumulative frequency of n=1485 measured cross-set heights. **D)** The cumulative frequency of n=51 measured flow depth proxies (i.e., barform heights, single channel storey heights).
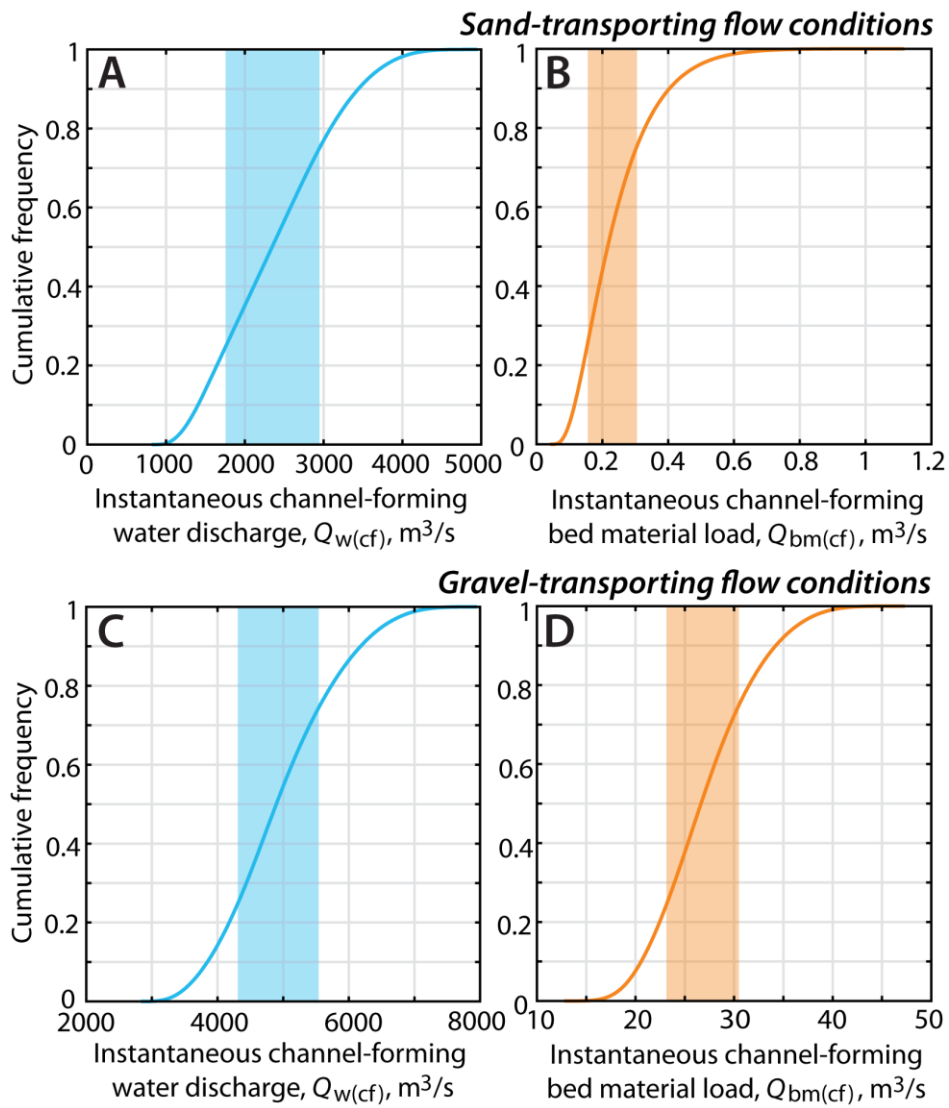
Figure 7: Field-derived estimates of **(A)** instantaneous channel-forming water discharges and **(B)** bed material load fluxes for sand-transporting flow condition. Field-derived estimates of **(C)** instantaneous channel-forming water discharges and **(D)** bed material load fluxes for gravel-transporting flow condition. Shaded regions indicate the 25th–75th percentiles of estimates.
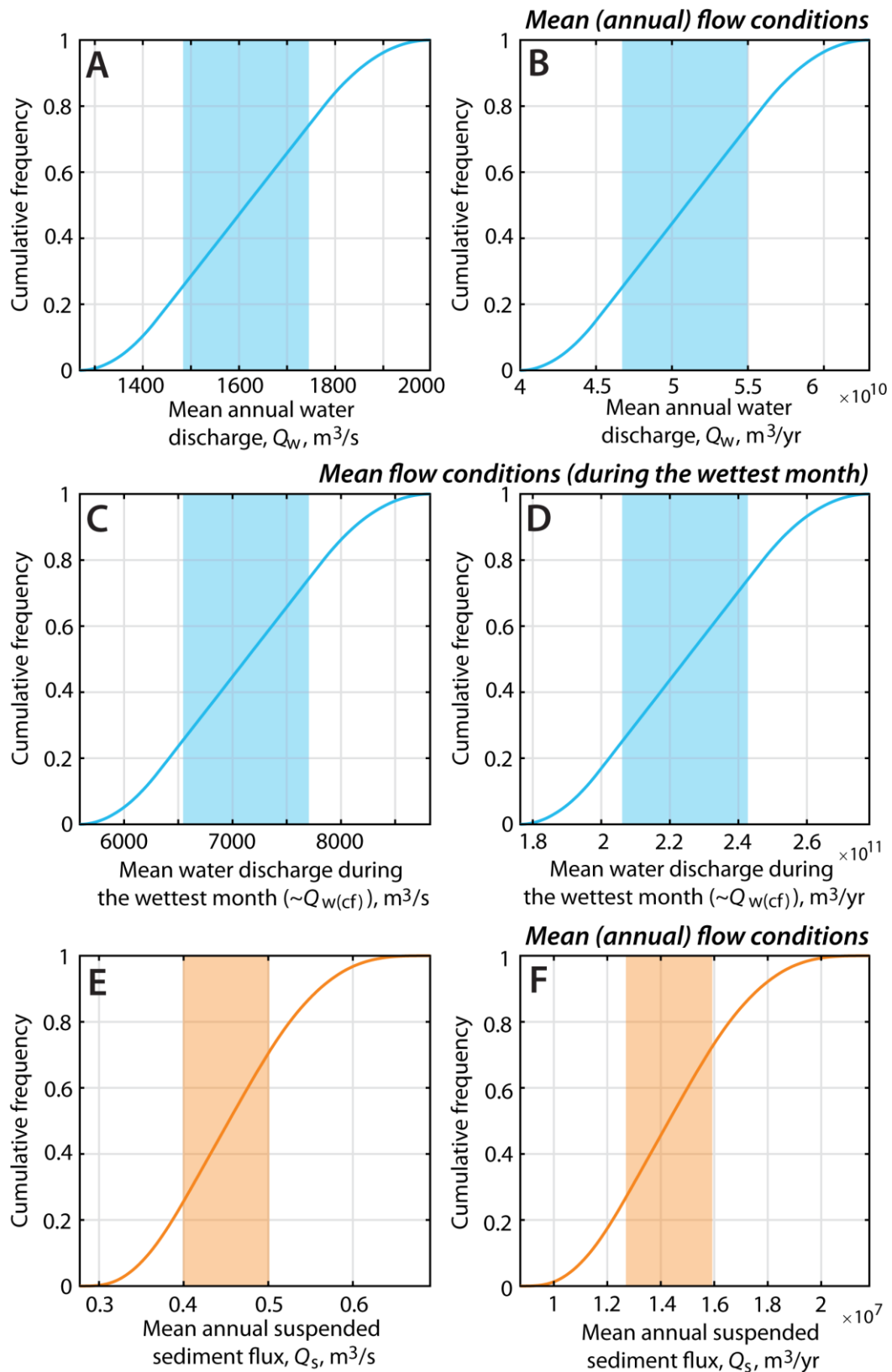
Figure 8: General circulation model (GCM)-derived estimates of water discharges and sediment fluxes. **A, B)** Mean annual water discharges in units of m³/s (part **A**) and m³/yr (part **B**). **C, D)** Mean water discharges during the wettest month of a simulated year in units of m³/s (part **C**) and m³/yr (part **D**). **E, F)** Mean annual suspended sediment fluxes in units of in units of m³/s (part **E**) and m³/yr. (part **F**). Shaded regions indicate the 25th–75th percentiles of estimates.
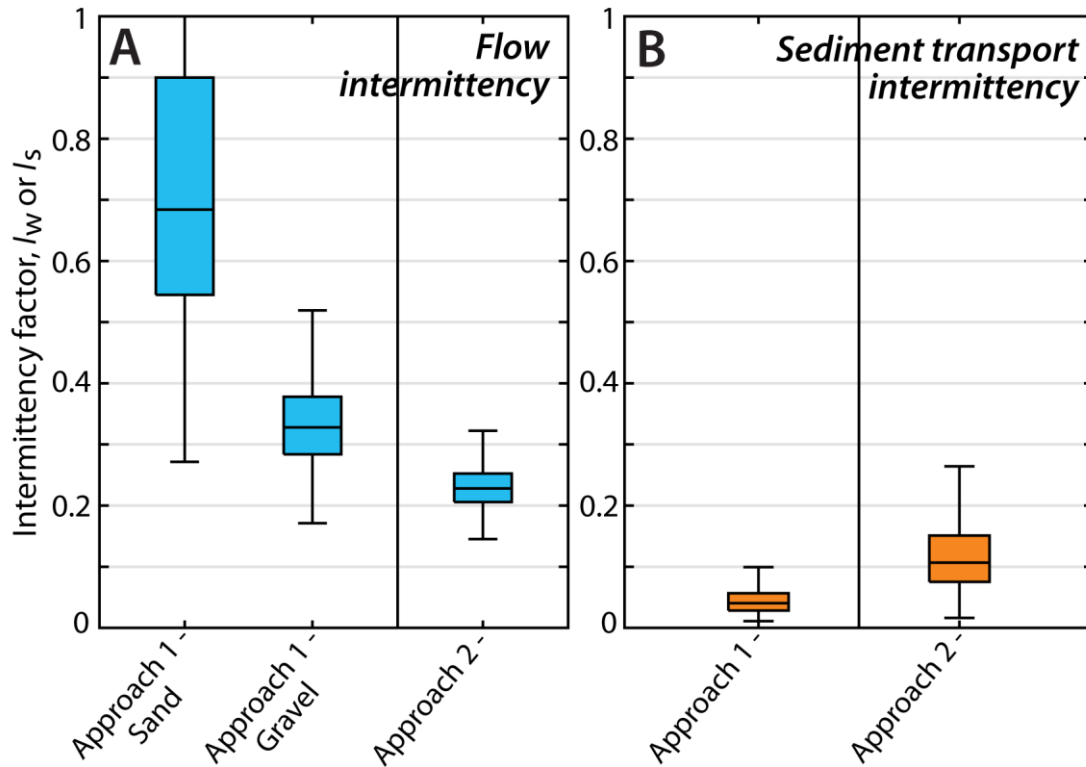
Figure 9: Estimated Intermittency factors in Last Chance Ferron rivers. **A)** Estimates of flow intermittency factors, I_w, were derived using Approach 1 for both sand-transporting flow conditions and gravel transporting flow conditions, respectively, and Approach 2. **B)** Estimates of sediment transport intermittency, I_s, were derived using Approach 1 (for sand-transporting flow conditions only) and Approach 2. The central mark of each box indicates the median estimate, and the bottom and top edges of each box indicate the 1st and 3rd quartiles (or 25th and 75th percentiles) of estimates, respectively. The whiskers of each box extend to the most extreme values that are not considered to be outliers (the extent of the whisker above $I_w=1$ in part **A** is not relevant; see Section 6.1 in the main text).

Table 1: Defining flow variability. We identify four principal timescales on which flow variability should be considered in geologic applications. These timescales reflect the timescales associated with various types of geologic field data and modelling approaches. We suggest that flow intermittency factors most closely reflect seasonal–interannual flow variability.

Timescale	Description (inc. spatial scale)	Potential metrics	Examples
Annual–decadal	This variability refers to trends in water discharge over years to decades and is often associated with climatic forcing on the same timescale, for example climate phenomena such as El Niño-Southern Oscillation and North Atlantic Oscillation. This variability is usually considered at catchment, regional, or continental spatial scales.	Flood frequency per year; peak annual discharge.	Simpson et al. (1993); Sun and Furbish (1997); Neal et al. (2002); Rîmbu et al. (2002); Pasquini and Depetris (2007); Das et al. (2013); Clark et al. (2014; Rood et al. (2016)
Seasonal–interannual	This variability refers to the shape and characteristics of the annual river hydrograph and considers the magnitudes and frequencies of discharge events. This variability is usually considered at catchment scales.	Precipitation seasonality index; discharge seasonality index; discharge peakedness.	Tachibana et al. (2008); Zhang et al. (2012); Juez et al. (2021)
Near-instantaneous	This variability refers to the shape and characteristics of hydrographs for individual discharge events. Discharge events may be flood events, however they do not have to be climatically forced and can also result from autogenic forcing, e.g., flow recession due to channel abandonment. This variability is usually considered at reach to catchment scales.	Total flood duration; rising limb duration; falling limb duration; total flood discharge; peak flood discharge; flood sediment transport capacity.	(Gaál et al., 2015); Najibi and Devineni (2017); Serinaldi et al. (2018); Liu et al. (2021)
Instantaneous	This variability refers to spatial heterogeneity of flow within a water column or channel cross-section.	Vertical flow velocity profile; horizontal flow velocity profile.	(Moramarco et al., 2011)

Table 2: Channel geometries, catchment geometries, and paleoclimates of the Last Chance Ferron paleocatchment. These values define the ranges implemented in Equations 1–8.

Input	Values used	Justification	References
Stratigraphic-based methods			
Sand fraction grain-size, D, m	0.0004–0.0011*	Primary field measurements of grain-size.	This study
Gravel fraction grain-size, D, m	0.006–0.01†	Primary field measurements of grain-size.	This study
Cross-set height, h_{xs}, m	0.06–0.28* 0.17–0.28†	Primary field measurements of cross-set heights	This study
Flow depth, H, m	2.84–8.80* 5.82–8.80†	Primary field measurements of bar-scale clinoform (lateral accretion set) heights and maximum thicknesses of single channel storeys. Secondary field measurements of lateral accretion set	This study (the data presented are the same as those presented in Lyster et al. (2022)); Cotter (1971); Garrison Jr and van den

		heights and maximum thicknesses of channel-fill deposits.	Bergh (2004); Gardner et al. (2004)
Flow width, W, m	200–300	Secondary field measurements and observations extracted from published literature	Bhattacharya and Tye (2004); Garrison Jr and van den Bergh (2004)
Bedform preservation ratio, h_{xs}/h_d	0.3–0.7	Evidence of enhanced bedform preservation in the Last Chance Ferron Sandstone.	Lyster et al. (2022)
Depositional volume, km³	430–530	Conversion of 2D depositional sequence stratigraphy (from Garrison Jr and van den Bergh (2004)) into 3D depositional volume using a 180° solid of revolution.	This study
Modelling-based methods			
Catchment area, A, km²	25,000–35,000	- Published paleogeographic reconstructions, including estimates of the catchment area and the distance between the paleoshoreline and drainage divide. - Previous investigation of paleocatchment configurations. - Theory of catchment outlet spacing.	Gardner (1995); Hovius (1996); Bhattacharya and Tye (2004); Ryer and Anderson (2004); Bhattacharya et al. (2016); Kynaston (2019); Lyster et al. (2020)
Catchment maximum relief, R, m	3,500–4,000	Published estimates of catchment relief based on structural restoration, paleofloral data, clumped isotope thermometry, and more.	Chase et al. (1998); DeCelles (2004); DeCelles and Coogan (2006); Sewall and Fricke (2013); Snell et al. (2014); Foreman et al. (2015); Lyster et al. (2020)
Catchment mean annual temperature, T, °C	11–18	HadCM3L general circulation model results	This study
Catchment mean annual precipitation, P, mm/yr	1600–1800	HadCM3L general circulation model results	This study
Catchment mean precipitation of wettest month, P, mm/yr	7050–7950	HadCM3L general circulation model results	This study

*The range of values is based on the mean (μ) and standard deviation (σ) of the observed or measured values. Specifically, the range is between μ− σ and μ+ σ. This range is used to estimate sand-transporting flow conditions.

†The range of values is based on the mean (μ) and standard deviation (σ) of the observed or measured values. Specifically, the range is between μ and μ+ σ. This range is used to estimate gravel-transporting flow conditions, with the specific purpose of simulating the largest formative flow conditions.

Supplement to: *Constraining flow and sediment transport intermittency in the geological past*

Sinéad J. Lyster[1,2,*], Alexander C. Whittaker[2], Alex Farnsworth[3] and Gary J. Hampson[2]

[1]Department of Geosciences, The Pennsylvania State University, Pennsylvania, USA.
[2]Department of Earth Science and Engineering, Imperial College London, UK.
[3]School of Geographical Sciences and Cabot Institute, University of Bristol, UK.
*slyster@psu.edu

<u>Contents:</u>

S1. Estimation of channel geometries
S2. Paleoflow conditions
S3. Uncertainty analysis
S4. HadCM3L General Circulation Model
S5. Field data

S1. Estimation of channel geometries

i.   Bedform heights

We used field measurements of dune-scale cross-set thicknesses, h_{xs}, to estimate mean original bedform (i.e., dune) heights, h_d. In doing so, we assumed the bedform preservation ratio, defined as the ratio of h_{xs} to h_d, i.e., h_{xs}/h_d, is a value between 0.3 and 0.7. Typically, h_{xs}/h_d is assumed to be a constant of ~0.3 in steady-state conditions, but can be up to 0.7 or higher in disequilibrium conditions (Paola & Borgman, 1991; Leclair & Bridge, 2001; Leclair, 2002; Jerolmack & Mohrig, 2005; Reesink et al., 2015; Ganti et al., 2020; Leary & Ganti, 2020). Lyster et al. (2022) presented evidence for enhanced bedform preservation under disequilibrium conditions in channel deposits of the Last Chance Ferron Sandstone, and we therefore assumed that h_{xs}/h_d can vary between 0.3 and 0.7 in our analyses.

ii.   Flow depths

To estimate flow depth, *H*, we used field measurements of select channel architectural elements as proxies for *H*. At field localities, which are reported in Table S1, we measured bar-scale clinoform heights and maximum thicknesses of single channel storeys (Tables S2 and S3). We also gathered data from literature (Tables S2 and S3). Where bar-scale clinoforms are fully preserved, they provide a minimum estimate for the maximum flow depth (e.g., Hajek & Heller, 2012). However, we note that measured bar-scale clinoforms were not necessarily fully-preserved, and may have been partially-preserved (c.f. Chamberlin and Hajek (2019)), and that our measurements do not account for compaction, which may add c. 10% to the estimated height (e.g., Allen, 1965). Importantly, we highlight that estimates of *H* derived from the heights of channel architectural elements have previously been corroborated using independent bedform-scale approaches to estimate *H* (c.f. Lyster et al., 2022).

iii.   Channel width

In the Last Chance Ferron Sandstone, the most paleo-landward localities preserve terrestrial fluvial deposits of major meandering trunk channels that fed the Last Chance fluvial-deltaic complex. For these deposits, Bhattacharya and Tye (2004) reported channel widths of 250 m. Further, Garrison Jr and van den Bergh (2004) noted that channels had average widths of 250 m, and that measured channel-belt widths did not exceed 2 km. These authors collectively found no evidence to suggest that channel widths in Last Chance

Ferron trunk channels exceeded a few hundred metres. To allow for uncertainty, we prescribed a range of channel widths spanning 200–300 m.

iv.   Paleoslope

To reconstruct paleoslope we used the empirical approach of Trampush et al. (2014) which, for sand-grade deposits, has been demonstrated to recover paleoslope values that are similar to paleoslope values recovered using a Shields stress inversion (Ganti et al., 2019; Lyster et al., 2021). Following Trampush et al. (2014), we estimated paleoslope, S, as

$$\log S = \alpha_0 + \alpha_1 \log D_{50} + a_2 \log H, \qquad\qquad \text{Eq. S1}$$

where $\alpha_0 = -2.08 \pm 0.036$, $\alpha_1 = 0.254 \pm 0.016$, and $\alpha_2 = -1.09 \pm 0.044$ are constants.

S2. Estimation of paleoflow conditions

i.   Flow characteristics

To calculate the instantaneous channel-forming water discharge, $Q_{w(cf)}$, and bed material load, $Q_{bm(cf)}$, we first calculated flow velocity, U, using the Chézy formulae for hydraulic flow resistance:

$$C_z \equiv \frac{U}{u_*} = C_f^{-\frac{1}{2}}, \qquad\qquad \text{Eq. S2}$$

where C_z is a Chézy friction coefficient, C_f is a dimensionless bed resistance coefficient, and $u*$ is the bed shear velocity ($u*=gHS^{0.5}$, where g is acceleration due to gravity). To solve for U, we calculated C_f using the Manning–Strickler formulation:

$$C_f^{-1/2} = \alpha_r \left(\frac{H}{k_s}\right)^{\frac{1}{6}}, \qquad\qquad \text{Eq. S3}$$

where α_r is a dimensionless constant between 8 and 9 and k_s is the skin friction height (or, the grain roughness height). For sand-bed streams $\alpha_r=8.32$ is often used (Wright & Parker, 2004). Meanwhile, k_s is approximated as $k_s \cong n_k D_{90}$, where n_k is a dimensionless number between 1.5 and 3 and D_{90} is the 90th percentile of grain-size. We assume $n_k=3$ following Wright and Parker (2004) and van Rijn (1984), and we substituted D_{50} for D_{90}, given the difficulty of measuring the D_{90} of sand-grade deposits in the field — we anticipate the effect of this assumption is negligible given that we implement generous uncertainty margins (see Section S3).

We then calculated instantaneous channel-forming water discharge, $Q_{w(cf)}$, as:

$$Q_{w(cf)} = UHW, \qquad\qquad \text{Eq. S4}$$

where U is the flow velocity, which we calculated using Chézy formulae (Equations S2 and S3), and where H and W were determined from primary and secondary field data, described previously.

ii.   Form drag correction

Equations S2 and S3 (and, therefore, S4) assume that all drag force exerted on the river bed is skin friction, i.e., they are skin friction predictors. In the absence of bedforms all drag force exerted on riverbeds is skin friction, however the presence of bedforms exerts additional form drag which acts normal to river beds. Use of a skin friction predictor is problematic as it acts to overestimate shear stress on the river bed (e.g.,

Andrews, 1984; Kean & Smith, 2006) and is in direct conflict with ubiquitous cross-bedding in terrestrial fluvial sandstone bodies of the Last Chance Ferron Sandstone.

In sediment transport models, form drag is accounted for analytically by "removing" the portion of flow depth affected by form drag. The flow depth of a river, H, can be considered a composite flow depth, H_c, which is the flow depth due to both skin friction and form drag. It is possible to calculate a skin friction flow depth, H_{sk}, which is the flow depth due to skin friction alone, i.e., the portion of the flow depth that is unaffected by form drag. The predictor of Wright and Parker (2004) is an empirical predictor of the Shields stress due to skin friction, τ^*_{sk}, where

$$\tau^*_{sk} = 0.05 + 0.7(\tau^* Fr^{0.7})^{0.8},$$ Eq. S5

and where Fr is the Froude number ($Fr = U/gH^{0.5}$). We solved for τ^*_{sk} iteratively. We iterated values of H_{sk} between 0 and H and for each value of H_{sk} we calculated: (1) the skin friction bed shear velocity, u^*_{sk}, as $u^*_{sk} = gH_{sk}S^{0.5}$; (2) the skin friction Shields stress, τ^*_{sk}, as $\tau^*_{sk} = H_{sk}S/RD_{50}$; (3) a constant T, as $T = (\tau^*_{sk} - 0.05/0.7)^{5/4}$; (4) the skin friction flow velocity, U_{sk}, using H_{sk} and Equations S1 and S2; and (5) the composite flow depth, H_c, as $H_c = (T(RD_{50}/S)(g^{0.5}/U_{sk})^{0.7})^{20/13}$. We iterated through values of H_{sk} until we found the value of H_{sk} such that H_c is equal to H. This methodology is outlined in detail in Parker (2004).

As k_s is a skin friction roughness height, we then calculated the composite roughness height, k_c, following Parker (2004) as

$$k_c = \frac{11H}{e^{\kappa Cz}},$$ Eq. S6

where κ is the von Karman constant, taken as 0.4, and where C_z is the skin friction C_z (Equation S1).

iii.   Suspended fraction of the bed material load

Prior to calculating the suspended fraction of the bed material load, we first calculated the sediment settling velocity, w_s, following Ferguson and Church (2004), as

$$w_s = \frac{RgD_{50}{}^2}{C_1 v + (0.75 C_2 RgD_{50}{}^3)^{0.5}},$$ Eq. S7

where C_1 and C_2 are constants associated with grain sphericity and roundness ($C_1 = 18$ and $C_2 = 1$ for natural grains; c.f. Ferguson and Church (2004)), and subsequently calculated the Rouse number, Z, as

$$Z = \frac{w_s}{\beta \kappa u_*}$$ Eq. S8

where β is a constant that correlates eddy viscosity to eddy diffusivity, typically taken as 1.

Several relations have been proposed to calculate the entrainment, E, of uniform material (see review by García and Parker (1991)), which is effectively the concentration of suspended sediment at the reference height or level, a. While various entrainment relations exist (e.g., van Rijn, 1984; García & Parker, 1991; Wright & Parker, 2004), we used the relation of Wright and Parker (2004) which best suits larger, low-sloping sand-bed rivers. Using the value of u^*_{sk} that resulted in $H_c = H$, Wright and Parker (2004) calculate entrainment as

$$E = \frac{AZ_u^5}{1 + \frac{A}{0.3}Z_u^5}, \qquad Z_u = \frac{u_{*sk}}{w_s} Re_p^{0.6} S^{0.7},$$ Eq. S9

where $A = 5.7 \times 10^{-7}$. We then computed the Rouse–Vanoni profile for suspended sediment as

$$I = \int_{\varsigma_b}^{1} \left[\frac{(1-\varsigma)/\varsigma}{(1-\varsigma_b)/\varsigma_b} \right]^Z \ln\left(30 \frac{H}{k_c} \varsigma\right) d\varsigma, \qquad \text{Eq. S10}$$

where b is a/H, and where $a = 0.05H$, so $b=0.05$. Finally, we calculated the instantaneous suspended fraction of the bed material load, $Q_{bm(s)}$, for channel-forming conditions in units of m²/s as

$$Q_{bm(s)} = \frac{u_* E H}{\kappa} I. \qquad \text{Eq. S11}$$

This framework recovers an instantaneous channel-forming discharge that is specific to the suspended bed material load, i.e., the portion of the bed material load that is intermittently suspended in the water column. It is not appropriate to refer to this value as a suspended sediment load. At present, the suspended bed material load has been reconstructed per unit width, which we multiplied by channel width, W, to recover the total suspended bed material load.

iv.   Bedload fraction of the bed material load

To calculate the instantaneous bedload fraction of the bed material load, $Q_{bm(b)}$, for channel-forming conditions, we used the relation of Mahon and McElroy (2018). This model is a bedform-scale model in which the unit bedload flux is calculated geometrically, per unit width. To implement this model, we first calculated the characteristic bedform migration velocity, V_c, prior to calculating the unit bedload flux (i.e., $Q_{bm(b)}$). These variables are given as:

$$\log V_c = \beta_0 + \beta_1 \log S, \qquad \text{Eq. S12}$$

$$Q_{bm(b)} = (1 - \varphi) \frac{h_d V_c}{2}, \qquad \text{Eq. S13}$$

where $\beta_0 = 0.6113 \pm 0.144$ and $\beta_1 = 1.305 \pm 0.0515$ are constants, and where φ is a dimensionless bed porosity of 0.5 (c.f. Mahon & McElroy, 2018). At present, the bedload fraction of the bed material load has been reconstructed per unit width, which we multiplied by channel width, W, to recover the total bedload fraction of the bed material load.

v.   Total bed material load

With estimates of both $Q_{bm(b)}$ and $Q_{bm(s)}$ for channel-forming conditions, we calculated the instantaneous channel-forming bed material load, $Q_{bm(cf)}$, as:

$$Q_{bm(cf)} = Q_{bm(b)} + Q_{bm(s)}. \qquad \text{Eq. S14}$$

S3. Uncertainty analysis

To account for variability and uncertainty in model inputs and parameters we implemented a Monte Carlo uncertainty propagation scheme. For each model input and parameter throughout Equations 1–8 in the main text, and in Equations S1–S14, we implemented a range of values. Specifically, we generated 10^6 random samples between bounds defined by this range. We generated samples from a uniform distribution in order to be as conservative as possible with uncertainty, and to avoid introduction of additional assumptions where the shape and the scale of the full distribution of the data is unknown (e.g., Equations S1 and S12). In propagating these randomly generated samples through Equations 1–8 and S1–S14, we recovered 10^6 plausible values for each reconstructed parameter and, therefore, we recovered 10^6 plausible values for the flow intermittency factor, I_w, and the sediment transport intermittency factor, I_s.

For model inputs that reflect field data, we determined this range using the mean (μ) and standard deviation (σ) of the data. We extracted μ and σ of sand-fraction grain-sizes, gravel-fraction grain-sizes, cross-set thicknesses, and channel architectural element thicknesses (i.e., flow depth proxies). For each of these datasets, we set bounds defined by μ and σ. To calculate sand-transporting flow conditions, which we interpreted as the dominant channel-forming condition (given the predominance of sand-grade deposits throughout channel-fill facies), these bounds were defined by $\mu - \sigma$ and $\mu + \sigma$. We interpreted gravel-transporting flow conditions as the least dominant channel-forming condition (due to the rare occurrence of gravel-grade deposits in channel-fill facies). However, we considered that gravel-transporting conditions potentially reflect the largest formative flow events preserved in the fluvial stratigraphy. To potentially simulate the largest formative flow events, we calculated gravel-transporting flow conditions using bounds defined by μ and $\mu + \sigma$.

Meanwhile, for model inputs that reflect topographic data, we determined this range based on independent observations or constraints in published literature, as outlined in the main text. Further, for paleoclimate data, we determined this range using results of HadCM3L simulations, which is also outlined in the main text. Finally, for model parameters in Equations S1 and S12, we defined the bounds for constants α_0, α_1, α_2, β_0, and β_1 as $\mu - \sigma$ and $\mu + \sigma$, using the values given for μ and σ.

S4. HadCM3L General Circulation Model

Here we employed HadCM3L, a coupled Atmosphere–Ocean General Circulation Model (AOGCM) similar to the widely used UKMO model HadCM3, but with a lower resolution ocean. HadCM3L (specifically HadCM3BL-M2.1aD; Valdes et al. (2017)) has a resolution of 3.75° longitude × 2.5° latitude in the atmosphere and ocean (equivalent to a cell size of 278 × 417 km at the equator and 278 × 295 km at 45° latitude), with 19 hybrid levels in the atmosphere and 20 vertical levels in the ocean with equations solved on the Arakawa B-grid with sub-grid scale processes (such as convection, cloud, orographic variance) parameterised. A dynamic vegetation model, TRIFFID (Top-down Representation of Interactive Foliage and Flora Including Dynamics; Cox et al. (1998)), predicts the life cycle and the distribution of vegetation using a plant functional type (PFT) approach for 5 different PFTs: broadleaf trees, needleleaf tree, C3 grass, C4 grass and shrubs. Grid-boxes are fractional and can contain a mixed coverage.

The model used in this study is very similar to the HadCM3BLM2.1aD model that is described and evaluated under modern climate configuration in Valdes et al. (2017), except that it includes a modification to the ozone profile which ensures that the model does not develop a runaway warming at ×4 preindustrial atmospheric CO_2, as discussed in Lunt et al. (2016). Relative to more recent and/or higher resolution GCMs, HadCM3L is fast and allows millennial and multi-millennial-scale integrations (Farnsworth et al., 2019), which is essential for deep-time modelling work where the initial condition may be far from the final equilibrium state. Recent work shows that deep-time GCMs require multi-thousand year integrations to fully represent applied boundary forcings (Farnsworth et al., 2019), and HadCM3L has been used successfully in numerous pre-Quaternary palaeoclimate studies (Lunt et al., 2007; Tindall et al., 2010; Craggs et al., 2012; Lunt et al., 2016).

Boundary conditions for the HadCM3L model used here are those described in Farnsworth et al. (2019), with boundary conditions (topography, bathymetry, ice sheet, solar luminosity) set for the Turonian stage of the Late Cretaceous. Turonian HadCM3L results are also identical to those presented in Farnsworth et al. (2019). Atmospheric CO_2 was set at 1120 ppmv (×4 preindustrial atmospheric CO_2), which is within the range of the Foster et al. (2017) reconstruction. The simulation was run for 11,422 model years and has reached full equilibrium with ocean integral temperatures showing insignificant trends and a top-of-the-atmosphere net energy balance of 0.1 W/m².

Results from Turonian HadCM3L simulations were resampled to a spatial resolution of 0.1° latitude × 0.1° longitude, which equates to a cell size of ~11 × 11 km, using a bilinear resampling technique. This facilitates visualization of spatial variation and enables selection of an appropriate range of values for paleoclimate variables required in this study.

S5. Field data

Table S1 | Field localities visited in this study

Locations	Elevation, m (±3–4)
N38 40 18.9, W111 24 52.5	2255
N38 40 20, W111 24 45.3	2241
N38 40 21.7, W111 24 17.1	2218
N38 40 17.5, W111 24 12	2209
N38 40 12, W111 24 2.5	2190
N38 40 7.7, W111 23 50.3	2179
N38 40 9.1, W111 23 44.8	2187
N38 40 8.9, W111 23 53.6	2215
N38 34 50.9, W111 28 6.2	2668
N38 34 49, W111 28 6.5	2636
N38 34 48.9, W111 28 4.5	2631
N38 34 47.6, W111 28 5.4	2592
N38 34 35.1, W111 27 48.4	2537
N38 44 0.4, W111 18 47.2	1965
N38 43 37.4, W111 18 46.5	1926
N38 43 25.2, W111 18 45.9	1895

Table S2 | Measured paleoflow depth indicators in terrestrial fluvial sandstone bodies of the Last Chance Ferron Sandstone. The data that are listed as sourced in this study are the same data as those presented in Lyster et al. (2022)

Paleoflow depth proxy	Thickness (m)	Source
Point bar deposit	9.1	Cotter (1971)
Point bar deposit	<8	Gardner et al. (2004)
Channel-fill deposits (maximum thickness)	~9	Gardner et al. (2004)
Channel-fill deposits (maximum thickness)	~9	Garrison Jr and van den Bergh (2004)
Point bar deposits	8, 7.5, 9, 3.2, 4.8, 3.6, 6.5, 7.5, 3.6, 4.1, 2.7, 6.4, 5.5, 2.8, 1.1, 1.9, 7.5, 2.7, 7.1, 1.2, 4.4, 3.7, 3.1, 3.4, 3, 2.5, 5.9, 2.5, 4.7, 10, 4.2, 1.6, 3, 6.5, 10	**This study/Lyster et al. (2022)**
Single channel storeys (maximum thickness)	8.6, 11.1, 12.2, 9, 7.6, 7.1, 3.9, 5.6, 2.6, 7.3, 12, 9.3	**This study/Lyster et al. (2022)**

Table S3 | Field data collected in this study. The table is located in the attached Excel spreadsheet in the sheet named "Data".

References

Allen, J. R. L. (1965). Fining-upwards cycles in alluvial successions. *Geological Journal, 4*(2), 229-246. DOI:10.1002/gj.3350040201

Andrews, E. D. (1984). Bed-material entrainment and hydraulic geometry of gravel-bed rivers in Colorado. *GSA Bulletin, 95*(3), 371-378. DOI:10.1130/0016-7606(1984)95<371:BEAHGO>2.0.CO;2

Bhattacharya, J. P., & Tye, R. S. (2004). Searching for Modern Ferron Analogs and Application to Subsurface Interpretation. In T. C. Chidsey, Jr., R. D. Adams, & T. H. Morris (Eds.), *Regional to Wellbore Analog for Fluvial-Deltaic Reservoir Modeling: The Ferron Sandstone of Utah* (Vol. 50, pp. 0). American Association of Petroleum Geologists. https://doi.org/10.1306/St50983

Chamberlin, E. P., & Hajek, E. A. (2019). Using bar preservation to constrain reworking in channel-dominated fluvial stratigraphy. *Geology, 47*(6), 531-534. DOI:10.1130/G46046.1

Cotter, E. (1971). Paleoflow characteristics of a late Cretaceous river in Utah from analysis of sedimentary structures in the Ferron sandstone. *Journal of Sedimentary Research 41*, 129–138. DOI:10.1306/74D72202-2B21-11D7-8648000102C1865D

Cox, P. M., Huntingford, C., & Harding, R. J. (1998). A canopy conductance and photosynthesis model for use in a GCM land surface scheme. *Journal of Hydrology, 212-213*, 79-94. DOI:10.1016/S0022-1694(98)00203-0

Craggs, H. J., Valdes, P. J., & Widdowson, M. (2012). Climate model predictions for the latest Cretaceous: An evaluation using climatically sensitive sediments as proxy indicators. *Palaeogeography, Palaeoclimatology, Palaeoecology, 315-316*(Supplement C), 12-23. DOI:10.1016/j.palaeo.2011.11.004

Farnsworth, A., Lunt, D. J., O'Brien, C., Foster, G. L., Inglis, G. N., Markwick, P., Pancost, R. D., & Robinson, S. A. (2019). Climate sensitivity on geological timescales controlled by non-linear feedbacks and ocean circulation. *Geophysical Research Letters, 0*(ja). DOI:10.1029/2019GL083574

Ferguson, R. I., & Church, M. (2004). A simple universal equation for grain settling velocity. *Journal of Sedimentary Research, 74*(6), 933-937. DOI:10.1306/051204740933

Foster, G. L., Royer, D. L., & Lunt, D. J. (2017). Future climate forcing potentially without precedent in the last 420 million years [Article]. *Nature Communications, 8*, 14845. DOI:10.1038/ncomms14845

Ganti, V., Hajek, E. A., Leary, K., Straub, K. M., & Paola, C. (2020). Morphodynamic hierarchy and the fabric of the sedimentary record. *Geophysical Research Letters, 47*(14), e2020GL087921. DOI:10.1029/2020GL087921

Ganti, V., Whittaker, A., Lamb, M. P., & Fischer, W. W. (2019). Low-gradient, single-threaded rivers prior to greening of the continents. *Proceedings of the National Academy of Sciences, 116*(4), 11652-11657. DOI:10.1073/pnas.1901642116

García, M., & Parker, G. (1991). Entrainment of Bed Sediment Into Suspension. *Journal of Hydraulic Engineering-asce - J HYDRAUL ENG-ASCE, 117*. DOI:10.1061/(ASCE)0733-9429(1991)117:4(414)

Gardner, M. H., Cross, T. A., & Levorsen, M. (2004). Stacking Patterns, Sediment Volume Partitioning, and Facies Differentiation in Shallow-Marine and Coastal-Plain Strata of the Cretaceous Ferron Sandstone, Utah. In T. C. Chidsey, Jr., R. D. Adams, & T. H. Morris (Eds.), *Regional to Wellbore Analog for Fluvial-Deltaic Reservoir Modeling: The Ferron Sandstone of Utah* (Vol. 50, pp. 0). American Association of Petroleum Geologists. https://doi.org/10.1306/St50983

Garrison Jr, J. R., & van den Bergh, T. C. V. (2004). High-Resolution Depositional Sequence Stratigraphy of the Upper Ferron Sandstone Last Chance Delta: An Application of Coal-Zone Stratigraphy. In T. C. Chidsey, Jr., R. D. Adams, & T. H. Morris (Eds.), *Regional to Wellbore Analog for Fluvial-Deltaic Reservoir Modeling: The Ferron Sandstone of Utah* (Vol. 50, pp. 0). American Association of Petroleum Geologists. https://doi.org/10.1306/St50983

Hajek, E. A., & Heller, P. L. (2012). Flow-depth scaling in alluvial architecture and nonmarine sequence stratigraphy: Example from the Castlegate Sandstone, central Utah, U.S.A. *Journal of Sedimentary Research, 82*(2), 121-130. DOI:10.2110/jsr.2012.8

Jerolmack, D. J., & Mohrig, D. (2005). Frozen dynamics of migrating bedforms. *Geology, 33*(1), 57-60. DOI:10.1130/G20897.1

Kean, J. W., & Smith, J. D. (2006). Form drag in rivers due to small-scale natural topographic features: 1. Regular sequences. *Journal of Geophysical Research: Earth Surface*, *111*(F4). DOI:10.1029/2006JF000467

Leary, K. C. P., & Ganti, V. (2020). Preserved fluvial cross strata record bedform disequilibrium dynamics. *Geophysical Research Letters*, *47*(2), e2019GL085910. DOI:10.1029/2019GL085910

Leclair, S. F. (2002). Preservation of cross-strata due to the migration of subaqueous dunes: an experimental investigation. *Sedimentology*, *49*(6), 1157-1180. DOI:10.1046/j.1365-3091.2002.00482.x

Leclair, S. F., & Bridge, J. S. (2001). Quantitative interpretation of sedimentary structures formed by river dunes. *Journal of Sedimentary Research*, *71*(5), 713-716. DOI:1527-1404/01/071-713/$03.00

Lunt, D., Farnsworth, A., Loptson, C., Foster, G., Markwick, P., O'Brien, C., Pancost, R. D., Robinson, S. A., & Wrobel, N. (2016). Palaeogeographic controls on climate and proxy interpretation. *Climate of the Past*, *12*, 1181-1198. DOI:10.5194/cpd-11-5683-2015

Lunt, D. J., Ross, I., Hopley, P. J., & Valdes, P. J. (2007). Modelling Late Oligocene C4 grasses and climate. *Palaeogeography, Palaeoclimatology, Palaeoecology*, *251*(2), 239-253. DOI:10.1016/j.palaeo.2007.04.004

Lyster, S. J., Whittaker, A. C., Hajek, E. A., & Ganti, V. (2022). Field evidence of bedform disequilibrium dynamics in preserved fluvial cross-strata: Discharge variability or morphodynamic hierarchy? *Earth and Planetary Science Letters*, *579*, 117355. DOI:10.1016/j.epsl.2021.117355

Lyster, S. J., Whittaker, A. C., Hampson, G. J., Hajek, E. A., Allison, P. A., & Lathrop, B. A. (2021). Reconstructing the morphologies and hydrodynamics of ancient rivers from source to sink: Cretaceous Western Interior Basin, Utah, USA. *Sedimentology*, *68*(6), 2854-2886. DOI:10.1111/sed.12877

Mahon, R. C., & McElroy, B. (2018). Indirect estimation of bedload flux from modern sand-bed rivers and ancient fluvial strata. *Geology*, *46*(7), 579-582. DOI:10.1130/G40161.1

Paola, C., & Borgman, L. (1991). Reconstructing random topography from preserved stratification. *Sedimentology*, *38*(4), 553-565. DOI:10.1111/j.1365-3091.1991.tb01008.x

Parker, G. (2004). *1D Sediment Transport Morphodynamics with Applications to Rivers and Turbidity Currents*.

Reesink, A. J. H., Van den Berg, J. H., Parsons, D. R., Amsler, M. L., Best, J. L., Hardy, R. J., Orfeo, O., & Szupiany, R. N. (2015). Extremes in dune preservation: Controls on the completeness of fluvial deposits. *Earth-Science Reviews*, *150*, 652-665. DOI:10.1016/j.earscirev.2015.09.008

Tindall, J., Flecker, R., Valdes, P., Schmidt, D. N., Markwick, P., & Harris, J. (2010). Modelling the oxygen isotope distribution of ancient seawater using a coupled ocean–atmosphere GCM: Implications for reconstructing early Eocene climate. *Earth and Planetary Science Letters*, *292*(3-4), 265-273. DOI:10.1016/j.epsl.2009.12.049

Trampush, S. M., Huzurbazar, S., & McElroy, B. (2014). Empirical assessment of theory for bankfull characteristics of alluvial channels. *Water Resources Research*, *50*(12), 9211-9220. DOI:10.1002/2014WR015597

Valdes, P. J., Armstrong, E., Badger, M. P. S., Bradshaw, C. D., Bragg, F., Crucifix, M., Davies-Barnard, T., Day, J. J., Farnsworth, A., Gordon, C., Hopcroft, P. O., Kennedy, A. T., Lord, N. S., Lunt, D. J., Marzocchi, A., Parry, L. M., Pope, V., Roberts, W. H. G., Stone, E. J., Tourte, G. J. L., & Williams, J. H. T. (2017). The BRIDGE HadCM3 family of climate models: HadCM3@Bristol v1.0. *Geoscientific Model Development*, *10*(10), 3715-3743. DOI:10.5194/gmd-10-3715-2017

van Rijn, L. C. (1984). Sediment transport, part II: Suspended load transport. *Journal of Hydraulic Engineering*, *110*(11), 1613-1641. DOI:10.1061/(ASCE)0733-9429(1984)110:11(1613)

Wright, S., & Parker, G. (2004). Flow resistance and suspended load in sand-bed rivers: Simplified stratification model. *Journal of Hydraulic Engineering*, *130*(8), 796-805. DOI:10.1061/(ASCE)0733-9429(2004)130:8(796)